



1 **Fluorescence characteristics, absorption properties, and**  
2 **radiative effects of water-soluble organic carbon in**  
3 **seasonal snow across northeastern China**

4 Xiaoying Niu<sup>1</sup>, Wei Pu<sup>1</sup>, Pingqing Fu<sup>2</sup>, Yang Chen<sup>1</sup>, Yuxuan Xing<sup>1</sup>, Dongyou Wu<sup>1</sup>,  
5 Ziqi Chen<sup>1</sup>, Tenglong Shi<sup>1</sup>, Yue Zhou<sup>1</sup>, Hui Wen<sup>1</sup>, Xin Wang<sup>1,2</sup>

6 <sup>1</sup>Key Laboratory for Semi-Arid Climate Change of the Ministry of Education, College of Atmospheric  
7 Sciences, Lanzhou University, Lanzhou 730000, China

8 <sup>2</sup>Institute of Surface-Earth System Science, Tianjin University, Tianjin 300072, China

9 *Correspondence to:* Xin Wang (wxin@lzu.edu.cn)

10 **Abstract.** Although water-soluble organic carbon (WSOC) in the cryosphere can significantly influence  
11 the global carbon cycle and radiation budget, WSOC in the snowpack has received little scientific  
12 attention to date. This study reports the fluorescence characteristics, absorption properties, and radiative  
13 effects of WSOC based on 34 snow samples collected from sites in northeastern China. Sampling sites  
14 were divided into five groups, comprising southeastern Inner Mongolia (SEIM), northeastern Inner  
15 Mongolia (NEIM), the south of northeastern China (SNC), the north of northeastern China (NNC), and  
16 the Changbai Mountain area (CBM). Together, these groups represent a significant degree of regional  
17 WSOC variability, with concentrations ranging from  $0.50 \pm 0.19$  to  $5.70 \pm 3.68 \mu\text{g g}^{-1}$  (mean =  $3.59 \pm$   
18  $3.19 \mu\text{g g}^{-1}$ ). We then identified the three principal fluorescent components of WSOC as (1) a  
19 high-oxygen humic-like component (HULIS-1) of terrestrial origin, (2) a low-oxygen humic-like  
20 component (HULIS-2) of mixed origin, (3) and a protein-like component (PRLIS) derived from  
21 autochthonous microbial activity. In SEIM, a region dominated by desert and exposed soils, the WSOC  
22 content exhibits the highest humification index (HIX) but the lowest fluorescence (FI) and biological  
23 (BIX) indices; the fluorescence signal is mainly attributed to HULIS-1, and thus implicates soil as the  
24 primary source. By contrast, the HIX (FI and BIX) value was the lowest (highest) and PRLIS most  
25 intense in the remote grasslands and forested areas of NEIM, suggesting a primarily biological source.  
26 For SNC and NNC, both of which are characterized by intensive agriculture and industrial activity, the  
27 fluorescence signal is dominated by HULIS-2 and the HIX, FI, and BIX values are all moderate,  
28 indicating mixed origins for WSOC (anthropogenic activity, microbial activity, and soil). We also  
29 observed that, throughout northeastern China, the light absorption of WSOC is dominated by HULIS-1,



1 followed by HULIS-2 and PRLIS. The contribution of WSOC to albedo reduction (average concentration  
2  $3.6 \mu\text{g g}^{-1}$ ) in the ultraviolet–visible (UV–vis) band is approximately half that of black carbon (BC:  
3 average concentration  $0.6 \mu\text{g g}^{-1}$ ); radiative forcing is  $3.8 (0.8) \text{ W m}^{-2}$  in old (fresh) snow, equating to  
4 19 % (17 %) of the radiative forcing of BC. These results indicate that WSOC has a profound impact on  
5 snow albedo and the solar radiation balance.

## 6 **1 Introduction**

7 Seasonal snow plays a significant role in Earth’s solar radiation energy budget owing to its high  
8 reflectivity (Beniston et al., 2017; Usha et al., 2020; Xie et al., 2018). In recent decades, however, the  
9 extent of snow-covered areas has trended downward, partially as a result of the presence of light-  
10 absorbing particles (LAPs) in the snowpack (Barnett et al., 2008; Groisman et al., 1994; Dumont et al.,  
11 2014; Keegan et al., 2014). Black carbon (BC), organic carbon (OC), mineral dust (MD), and biota  
12 comprise the principal light-absorbing particles in seasonal snow (Di Mauro, 2020; Qian et al., 2015),  
13 which together serve to lower surface albedo and impose a positive radiative forcing (Dumont et al.,  
14 2014; Hansen and Nazarenko, 2004; Warren and Wiscombe, 1980; Zhang et al., 2017). Concurrently,  
15 LAPs absorb solar radiation, thereby accelerating snow melt (Li et al., 2021b). Ultimately, the disruption  
16 of the global radiative balance due to LAPs has important implications for regional and global climate  
17 change (Skiles et al., 2018).

18 Snowpack BC and MD have been the focus of considerable research in snow-covered regions worldwide  
19 (Li et al., 2021a; Zhang et al., 2018; Antony et al., 2014; Hegg et al., 2010; Doherty et al., 2014; Wang  
20 et al., 2015). As the most important LAP (Bond et al., 2013; Doherty et al., 2010; Wang et al., 2014b),  
21 the radiative efficiency of snowpack BC can be more than three times greater than that of carbon dioxide  
22 (Flanner et al., 2007), and MD, another important snowpack LAP, is also known to alter the cryospheric  
23 environment owing to its light-absorbing properties (Di Mauro et al., 2015; Painter et al., 2007; Sarangi  
24 et al., 2020; Shi et al., 2021). Recently, researchers have also begun evaluating the influence of biomes  
25 on global snow albedo (Hotaling et al., 2021). In contrast, however, the role of OC remains poorly  
26 understood because of its complex composition and a relative dearth of OC-focused research.  
27 Consequently, substantial uncertainty surrounds the origins, optical properties, and radiative effects of  
28 snowpack OC.



1 A recent study has reported that the storage of OC in mountain glaciers and ice caps (~11 % of Earth's  
2 land surface) could be as high as 6 petagrams (Pg; Hood et al., 2015), the majority of which is water-  
3 soluble organic carbon (WSOC). WSOC is one of the largest sources of bioavailable organic carbon in  
4 aquatic ecosystems (Battin et al., 2009). Moreover, as the chief absorber of WSOC, water-soluble brown  
5 carbon (WS-BrC) can absorb significant measures of solar radiation in the ultraviolet–visible (UV–vis)  
6 wavelengths (Murphy et al., 2008). For instance, in their analysis of 21 snow samples from Arctic and  
7 Antarctic, Anastasio and Robles (2007) observed that 50 % of the total light absorption coefficients at  
8 wavelengths > 280 nm might be attributed to organic chromophores of WSOC. In surficial snow samples  
9 from Barrow, Alaska, Beine et al. (2011) reported that WSOC occupies almost the entire absorption  
10 spectrum of the photochemically active region (300–450 nm), and Feng et al. (2016) observed that  
11 absorption in cryoconite samples from the central Tibetan Plateau is dominated by WSOC components  
12 in the 300–350 nm range. Similarly, Yan et al. (2016) measured WSOC in glacial snow from Laohugou,  
13 northern Tibetan Plateau, where they found that the radiative forcing is ~10 % that of BC. Together,  
14 these studies indicate that WSOC plays a key role in global snowpack energy absorption (Niu et al., 2018;  
15 Zhang et al., 2020). Nevertheless, we note that previous research on cryospheric WSOC has focused  
16 largely on alpine glaciers and polar regions; the extensive mid-latitude regions impacted by seasonal  
17 snowpack remain relatively understudied.

18 The composition of WSOC is typically complex, and characteristics of fluorescence and absorption can  
19 vary widely among the different components. Nonetheless, recent studies have tended to treat WSOC as  
20 a single entity and focus on the overall impacts, such that the specific roles of individual components are  
21 poorly constrained. One commonly used analytical method for distinguishing the components and  
22 properties of fluorescence is the fluorescence excitation-emission matrix (EEM), which has the  
23 advantage of high sensitivity and small sample size (Coble, 1996; Kowalczyk et al., 2005). First applied  
24 in oceanic contexts (Coble et al., 1990), EEM has been gradually extended to lakes, fog water, rainwater,  
25 and atmospheric aerosols in addition to glacial meltwater, ice cores, and snow (Birdwell and Valsaraj,  
26 2010; Huguet et al., 2009; McKnight et al., 2001). Concurrently, parallel factor analysis (PARAFAC) is  
27 an effective approach for extracting from complex EEMs the individual fluorescence components and  
28 their corresponding fluorescence information, thus making EEM–PARAFAC a direct and viable means  
29 for exploring sources of WSOC. For example, Zhou et al., (2019b) used EEM–PARAFAC to identify



1 the multiple sources of WSOC measured in seasonal snow in northwestern China. Accordingly, we have  
2 applied EEM–PARAFAC in our analysis of snow samples for this study.  
3 Northeastern China supports an extensive snowpack during winter and spring. As a major industrial and  
4 agricultural center, this region is also the principal source of heavy airborne pollutants that are  
5 incorporated into seasonal snow via wet and dry deposition (Wang et al., 2017). Coupled with intensive  
6 tilling of farmland, the geographical proximity of northeastern China to neighboring desert regions also  
7 provides a source of soil organic matter that becomes entrained into the snowpack (Wang et al., 2013b).  
8 Compared with research on BC-snow mixing ratios and their radiative impact in northeastern China  
9 (Dang et al., 2017; Huang et al., 2011; Pu et al., 2019), studies of WSOC are still in their infancy. To  
10 address this deficiency, we analyzed 34 samples of seasonal snow collected in December 2020 and  
11 January 2021 to make the first investigation of the fluorescence characteristics, absorption properties,  
12 and radiative effects of WSOC in northeastern China. Specifically, we applied EEM–PARAFAC to  
13 identify the origins and fluorescence characteristics of snowpack WSOC, after which we derived  
14 individual absorption contributions for each WSOC component using fluorescence data, an absorption  
15 data series, and an attribution method. Finally, we estimated the reduction of snow albedo and radiative  
16 forcing caused by WSOC and BC via the Spectral Albedo Model for Dirty Snow (SAMDS) radiative  
17 transfer model.

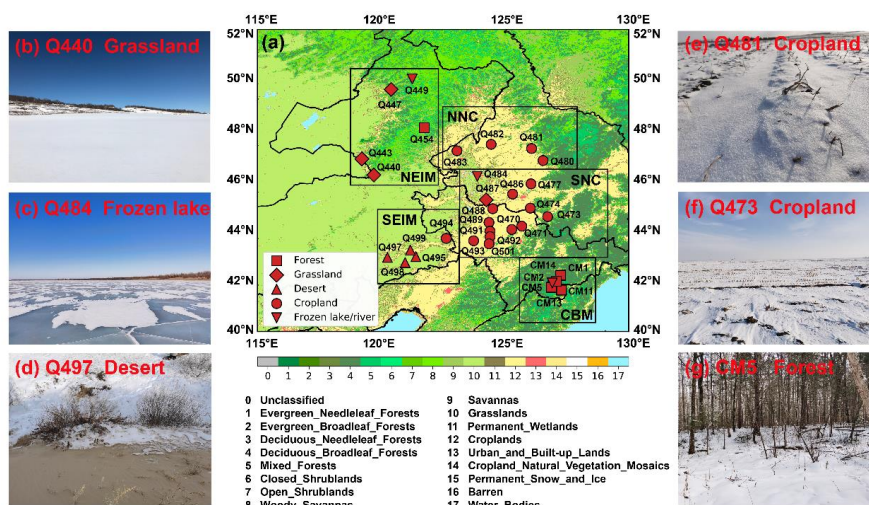
## 18 **2 Methods**

### 19 **2.1 Sample collection**

20 During the months of January and December 2020 and January 2021, we collected 34 snow samples  
21 from sites across northeastern China, including the eastern part of Inner Mongolia and Heilongjiang and  
22 Jilin provinces. Sample numbers were set following previous campaigns (Pu et al., 2017; Wang et al.,  
23 2013b, 2017), with the exception that samples from the Changbai Mountain area are numbered  
24 individually. The geographical distribution of sampling sites and respective land-cover types are shown  
25 in Figure 1a; our sites are characterized by five land-cover types, including forest, grassland, desert,  
26 cropland, and frozen lake/river (Fig. 1b–g). On the basis of these geographical and environmental  
27 classifications, we divided the sampling sites into five broad regions: southeastern Inner Mongolia (SEIM;  
28 Q494–495, Q497–499), the south of northeast China (SNC; Q470–471, Q473–474, Q477, Q484, Q486–



- 1 Q489, Q491–Q493, Q501), the north of northeast China (NNC; Q480–483), the Changbai Mountain
- 2 area (CBM; CM1–CM2, CM5, CM11, CM13–CM14), and northeastern Inner Mongolia (NEIM; Q440,
- 3 Q443, Q447, Q449, Q454).



4  
 5 **Figure 1:** (a) Information on sampling site distributions in northeastern China, including the land cover type,  
 6 site number, and grouping. Land cover types are derived from Collection 5.1 of the MODIS global land cover  
 7 type dataset (MCD12Q1: <https://lpdaac.usgs.gov/products/mcd12q1v006/>) and are indicated by specific  
 8 colors and symbols relative to sampling sites. Sampling sites are divided into the five groups defined by black  
 9 rectangles. (b–g) Photographs depicting the typical snow and ground-cover conditions of our various sampling  
 10 sites.

11 Our sample sites were chosen at random but had to be located  $\geq 20$  km from cities and villages and at  
 12 least a kilometer upwind of roads or railroads to minimize the influence of single-point pollution sources  
 13 and to ensure the broadest regional representation. Furthermore, we performed sample collection oriented  
 14 toward the wind to avoid contamination from personnel. At each site, we used a sterile disposable shovel  
 15 to collect 0–5 cm-thick samples of surface snow, which were subsequently stored in sterile Whirlpak  
 16 (Nasco, WI, USA) bags. For snow depths  $< 5$  cm, we determined the sampling depth according to the  
 17 actual conditions to avoid inducing significant soil impurities during sampling. Snow samples were  
 18 melted at room temperature (25 °C) and stored in a freezer at  $-20$  °C until analysis in the laboratory. For  
 19 more operational details, we refer the reader to Wang et al. (2013b).



## 1 2.2 Chemical species analysis

2 After collection, samples were melted at room temperature (25 °C) before being filtered using a  
3 disposable sterile syringe (Jiangnan, Anhui, China) and 0.45 µm pore-sized polytetrafluoroethylene  
4 (PTFE) filter (Jingteng, Tianjin, China) (Chen et al., 2019a). Prior to analysis, filtrates were stored in  
5 pre-baked (4 hours at 450 °C) glass vials in a freezer. For each sample, we used a total organic carbon  
6 analyzer (Aurora 1030W, OI Analytical, TX, USA) to measure the concentration of WSOC;  
7 measurement detection limits and relative standard deviations were 2 µg L<sup>-1</sup> and 1 %, respectively.  
8 Blank-corrected concentrations are provided in Table S1.

9 We used 0.4 µm pore-sized polycarbonate filter membranes (Whatman, USA) to isolate BC and other  
10 insoluble particles, following the protocols outlined by Shi et al. (2020) and Wang et al. (2014b), after  
11 which we employed a custom-developed two-sphere integrating-sandwich (TSI) filter-based  
12 spectrophotometer to measure particle absorption. Coupled with the mass of filtered meltwater, these  
13 optical measurements were then converted to snowpack BC concentrations. To make these calculations,  
14 we applied a BC mass-absorption coefficient (MAC) and absorption Ångström exponent (AAE) of 6.3  
15 m<sup>2</sup> g<sup>-1</sup> (550 nm) and 1.1, respectively, after Pu et al. (2017). We note that TSI provides greater accuracy  
16 and smaller overall uncertainties in the quantification of seasonal snow BC than do thermo-optical carbon  
17 analysis (Wang et al., 2020), and thus it has been applied widely in this type of research (Shi et al., 2020).  
18 For more detailed information, we refer the reader to Wang et al. (2013b).

## 19 2.3 Fluorescence and absorption measurement

20 We obtained absorbance and fluorescence EEMs for filtered meltwater samples via synchronous  
21 absorption-3D Fluorescence scanning spectrometry (Aqualog, Horiba Scientific) with the following  
22 measurement parameters: excitation = 240–800 nm in 3 nm intervals; emission = 152.25–929.92 nm in  
23 5.04 nm (8 pixels) intervals; scanning interval = 0.3 seconds. Prior to sample measurement, we analyzed  
24 aliquots of filtered ultra-pure water (18.2 M Ω cm, Milli-q Purification System, Millipore) as analytical  
25 blanks. We normalized fluorescence intensity to that of the water Raman unit (RU), which exhibits a  
26 peak excitation wavelength of 350 nm, and deducted this Raman signal from all subsequent sample tests  
27 (Lawaetz and Stedmon, 2009). The inner filtration effect and Rayleigh scattering peaks were also  
28 dispelled following the methods reported by Kothawala et al. (2013) and Bahram et al. (2006),  
29 respectively. As fluorescence spectra with wavelengths greater than 600 nm are primarily noise (Zhou et



1 al., 2019b), they are not considered further in this study. Likewise, any samples with absorption spectra  
2 of >600 nm wavelengths were subtracted for the baseline correction (Chen et al., 2019b).

3 We used version 0.6.3 of the MATLAB drEEM toolbox (<http://dreem.openfluor.org/>; Murphy et al.,  
4 2013) to perform PARAFAC analysis on EEMs. Comprising the consistency index, residuals, and visual  
5 inspections, the 3-component model is considered more reliable and representative than are the 2–7-  
6 component models (Fig. S1 in the Supplement) and passes the S4C6T3 split scheme (Fig. S2; Murphy  
7 et al., 2013). The contributions of these three components to the overall fluorescence signal are expressed  
8 as relative percentages of  $F_{\max}$  in RU, and the total fluorescence volume (TFV; RU nm<sup>2</sup>) is calculated  
9 from the EEMs (Song et al., 2019). Normalized TFV equates to NFV (RU nm<sup>2</sup> (mg L<sup>-1</sup>)<sup>-1</sup>), TFV  
10  $c(\text{WSOC})^{-1}$ , where  $c(\text{WSOC})$  is the concentration of WSOC in the snow (mg L<sup>-1</sup>), and represents a  
11 sample's fluorescence ability (Chen et al., 2019a).

12 We calculated three fluorescence-derived indices—the fluorescence index (FI), biological index (BIX),  
13 and humification index (HIX)—from the ratio of fluorescence intensity at specific excitation and  
14 emission wavelengths. As demonstrated by previous studies (Birdwell and Valsaraj, 2010; Huguet et al.,  
15 2009; McKnight et al., 2001), these ratios can help characterize potential sources of WSOC. Specifically,  
16 the FI is taken to represent the relative amount of DOM derived from terrestrial and microbial/algae  
17 sources (McKnight et al., 2001); high values correspond to terrestrially derived organics, and low values  
18 reflect microbial sources. The HIX describes the degree of humification of soluble organic matter  
19 (Zsolnay et al., 1999). During humification, the aromaticity of organic matter increases as microbial  
20 availability decreases, such that higher HIX values correspond to more strongly humified and/or higher  
21 aromaticity organics (principally of terrestrial origin), whereas lower values indicate autochthonous or  
22 microbial origins. As a measure of autochthonous productivity (Huguet et al., 2009), elevated BIX values  
23 are associated with increased contributions of microbial-derived fluorescent organic matter. The three  
24 indices are calculated by the following equations (Ohno, 2002; Huguet et al., 2009; McKnight et al.,  
25 2001; Feng et al., 2016):

$$26 \quad FI = \frac{I(Ex = 370, Em = 470)}{I(Ex = 370, Em = 520)} \quad (1)$$

$$27 \quad BIX = \frac{I(Ex = 310, Em = 380)}{I(Ex = 310, Em = 430)} \quad (2)$$

$$28 \quad HIX = \frac{I(Ex = 254, Em = 435 - 480)}{I(Ex = 254, Em = 300 - 345) +} \quad (3)$$



1 where  $I$  is the fluorescence intensity, and  $\lambda_{ex}$  and  $\lambda_{em}$  represent the excitation and emission wavelengths,  
2 respectively. To ensure a direct comparison with prior results, we recalculated published HIX data using  
3 the same calculation methods as in our own analyses.

4 We converted sample absorbance to an absorption coefficient using the following equation:

$$5 \quad a_{WSOC}(\lambda) = \ln(10) \cdot Abs(\lambda)/L \quad (4)$$

6 where  $Abs$  is absorbance,  $\lambda$  is wavelength,  $L$  is the path length of the cuvette (0.01 m), and  $a_{WSOC}$  is the  
7 absorption coefficient ( $m^{-1}$ ).

8 Owing to the absorption characteristics of WSOC, we selected the absorption coefficient at 280 nm  
9 ( $a_{WSOC}(280)$ ) to characterize the absorption intensity of WSOC.

10 To investigate the wavelength dependence of WSOC absorption, we obtained the Absorption Ångström  
11 exponent (AAE) via the following equation (Doherty et al., 2010; Niu et al., 2018; Wang et al., 2013b;  
12 Yan et al., 2016):

$$13 \quad a_{WSOC}(\lambda) = K \cdot \lambda^{-AAE} \quad (5)$$

14 where  $K$  is a constant related to WSOC concentration.

15 We calculated the mass absorption coefficient ( $MAC_{\lambda}$ ,  $m^2 g^{-1}$ ) of our samples using the equation (Chen  
16 et al., 2019b; Yan et al., 2016):

$$17 \quad MAC_{\lambda} = a_{WSOC}(\lambda) / c(WSOC) \quad (6)$$

18 where  $a_{WSOC}$  is the absorption coefficient derived from Equation (4) and  $c(WSOC)$  ( $mg L^{-1}$ ) is the  
19 concentration of WSOC.

#### 20 **2.4 Snow albedo modeling and radiative forcing calculations**

21 To establish the radiative effect impact of snowpack WSOC in northeastern China, we used SAMDS to  
22 simulate spectral snow albedo. This model is based on asymptotic radiative transfer theory, which has  
23 been verified by previous studies (Li et al., 2021b; Wang et al., 2017) and described in detail by Wang  
24 et al. (2017), and it involves parameters including solar zenith angle, impurity concentrations, snow  
25 radius, and equivalent particle size. Measured values include the concentration of BC and absorption  
26 coefficients of WSOC. To quantify the influence of pollutants on snow albedo, we assumed a semi-  
27 infinite snow layer and uniform snow grain radii of 100  $\mu m$  for fresh snow and 1000  $\mu m$  for old snow,

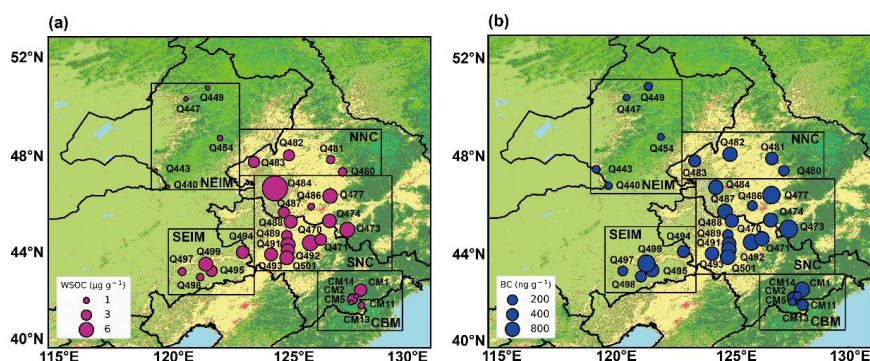


1 consistent with previous studies (Pu et al., 2021). With the solar zenith angle fixed at  $60^\circ$ , in line with  
2 our sampling dates and locations, we calculated the reduction in spectral snow albedo for the UV–vis  
3 (280–400 nm) and ultraviolet–near infrared (UV–NIR; 280–1500 nm) bands. Radiative forcing was then  
4 derived by multiplying the albedo reduction value by the incident solar radiation (Painter et al., 2013),  
5 permitting us to evaluate radiative forcing under four scenarios: pure snow, WSOC only, BC only, and  
6 WSOC + BC.

### 7 3 Results and discussion

#### 8 3.1 Characteristics of chemical species

9 Figure 2a shows the spatial distribution of measured WSOC in seasonal snow across northeastern China.  
10 Averaged across our entire study area, the mean WSOC concentration (arithmetic mean  $\pm$  standard  
11 deviation) is  $3.59 \pm 3.19 \mu\text{g g}^{-1}$ , with a maximum of  $17.99 \mu\text{g g}^{-1}$  and a minimum of  $0.29 \mu\text{g g}^{-1}$ . Among  
12 the five regions, WSOC concentrations are highest in SNC (average  $5.7 \pm 3.68 \mu\text{g g}^{-1}$ ), likely reflecting  
13 the greater degree of agricultural and industrial activity there compared with other regions (Lu et al.,  
14 2011; Wang et al., 2013b). We highlight that both agricultural and industrial sources are considered  
15 anthropogenic. In contrast, our second highest measured concentrations ( $3.35 \pm 1.49 \mu\text{g g}^{-1}$ ) are from  
16 SEIM, where desertification occurs (Fang et al., 2007) and is therefore considered a natural source of  
17 WSOC. For most sites, the underlying surface is desert (Fig. 1a) that was incompletely covered by  
18 seasonal snow during the sampling period (Fig. 1d). Consequently, the exposure of natural sandy soils is  
19 a potentially significant contributor of WSOC through aeolian erosion and dry deposition.



20  
21 **Figure 2: Spatial distributions of concentrations of (a) WSOC and (b) BC in snow samples. Sampling sites are**  
22 **divided into the five groups defined in Figure 1. Bubble sizes are proportional to concentrations of WSOC**  
23 **and BC.**



1 In NNC, where both the population density and agricultural intensity are lower than in SNC (Choi et al.,  
2 2020), the contribution of anthropogenic pollution to snowpack is correspondingly lower, resulting in a  
3 moderate WSOC concentration of  $2.7 \pm 0.75 \mu\text{g g}^{-1}$ . Meanwhile, far from intensive human activity, both  
4 CBM and NEIM (Fig. 1a, b, and g) returned low WSOC concentrations (CBM:  $1.95 \pm 1.28 \mu\text{g g}^{-1}$ ; NEIM:  
5  $0.50 \pm 0.19 \mu\text{g g}^{-1}$ ). Nonetheless, the higher value for CBM betrays the influence of far-traveled  
6 anthropogenic pollutants (Wu et al., 2020; Zhang et al., 2013).

7 In comparison with previous studies, we observed that, with the exception of NEIM, our measured  
8 WSOC concentrations are significantly higher than those reported for snow/ice from the Tibetan Plateau  
9 (TGL;  $\sim 0.71\text{--}1.02 \mu\text{g g}^{-1}$ ; Feng et al., 2016), the Alps ( $\sim 0.14\text{--}0.78 \mu\text{g g}^{-1}$ ; Vione et al., 2021), North  
10 America ( $\sim 0.1\text{--}0.3 \mu\text{g g}^{-1}$ ; Fellman et al., 2015), and polar regions ( $\sim 0.12\text{--}0.27 \mu\text{g g}^{-1}$ ; Antony et al.,  
11 2014), but comparable to values in Laohugou glacier ice from the Tibetan Plateau ( $\sim 1.02\text{--}2.6 \mu\text{g g}^{-1}$ ;  
12 Feng et al., 2018, 2016) and seasonal snowpack in northwestern China ( $0.48\text{--}7.07 \mu\text{g g}^{-1}$ ; Zhou et al.,  
13 2021). This finding implies that snowpack WSOC in northeastern China is contributing significantly to  
14 regional and global climate change (Domine, 2002).

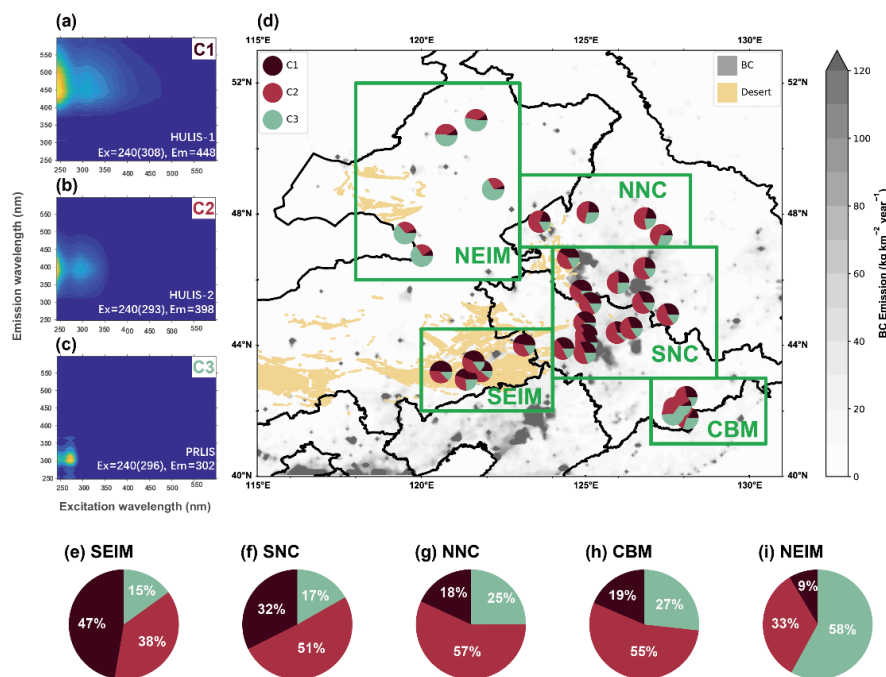
15 A similar spatial pattern is exhibited by snowpack BC (Fig. 2b). For example, of all five regions, the  
16 regional mean BC concentration is highest for SNC (mean:  $922.99 \pm 512.10 \text{ ng g}^{-1}$ ), followed by SEIM  
17 ( $659.17 \pm 581.85 \text{ ng g}^{-1}$ ), NNC ( $494.13 \pm 223.81 \text{ ng g}^{-1}$ ), and the CBM ( $391.38 \pm 312.49 \text{ ng g}^{-1}$ ). BC  
18 concentrations are lowest in NEIM ( $59.79 \pm 18.68 \text{ ng g}^{-1}$ ), in agreement with the values in remote areas  
19 reported by Doherty et al. (2010).

### 20 3.2 Fluorescence characteristics of WSOC

21 Three fluorescent components (C1–C3) were captured by resolving the EEMs spectra; all fluorescence  
22 information is summarized in Table S2. C1 exhibits a primary peak at  $\text{Ex} = 240 \text{ nm}$ ,  $\text{Em} = 448 \text{ nm}$ ,  
23 indicating a high-oxygenated HULIS found primarily in aromatic conjugated macromolecules (Chen et  
24 al., 2016). The weaker secondary peak occurs at longer excitation wavelengths ( $\text{Ex} / \text{Em} = 308 / 448 \text{ nm}$ ),  
25 implying a higher aromatic content and greater molecular weight (Coble et al., 1998). Wen et al. 2021  
26 concluded that C1 is probably derived from natural terrestrial sources, such as dust and soil, as proposed  
27 originally by Stedmon et al. (2003) and Osburn et al. (2016). Accordingly, we classified C1 as a terrestrial,  
28 humic-like substance, hereafter referred to as HULIS-1.



1 C2 exhibits a primary (secondary) peak at Ex = 240 (293) nm, Em = 398 nm, suggestive of  
 2 lower-oxygenated HULIS (Chen et al., 2016). Observed in a variety of sources, Stedmon et al. (2003)  
 3 reported this component in terrestrial end-member samples, whereas both Murphy et al. (2011) and  
 4 Osburn et al. (2016) have since linked C2 to anthropogenic sources, such as urban runoff and sewage.  
 5 Microbial activity and the degradation of phytoplankton in natural aquatic systems are also thought to  
 6 contribute to this component (Yamashita et al., 2008; Zhang et al., 2009). Accordingly, we classified C2  
 7 as humic-like substances with complex origins in terrestrial, anthropogenic, and/or microbial sources,  
 8 hereafter termed HULIS-2. Unlike HULIS-1 and HULIS-2, C3 is recognizable as a UVB-like protein or  
 9 tyrosine-like fluorescence (hereafter PRLIS) with a primary (secondary) peak at Ex = 240 (293) nm, Em  
 10 = 398 nm (Osburn et al., 2016; Stedmon and Markager, 2005). PRLIS reflects autochthonously labile  
 11 DOM produced by biological processes (Stedmon et al., 2003) and has been reported in previous studies  
 12 of seasonal snow (Zhou et al., 2019b).



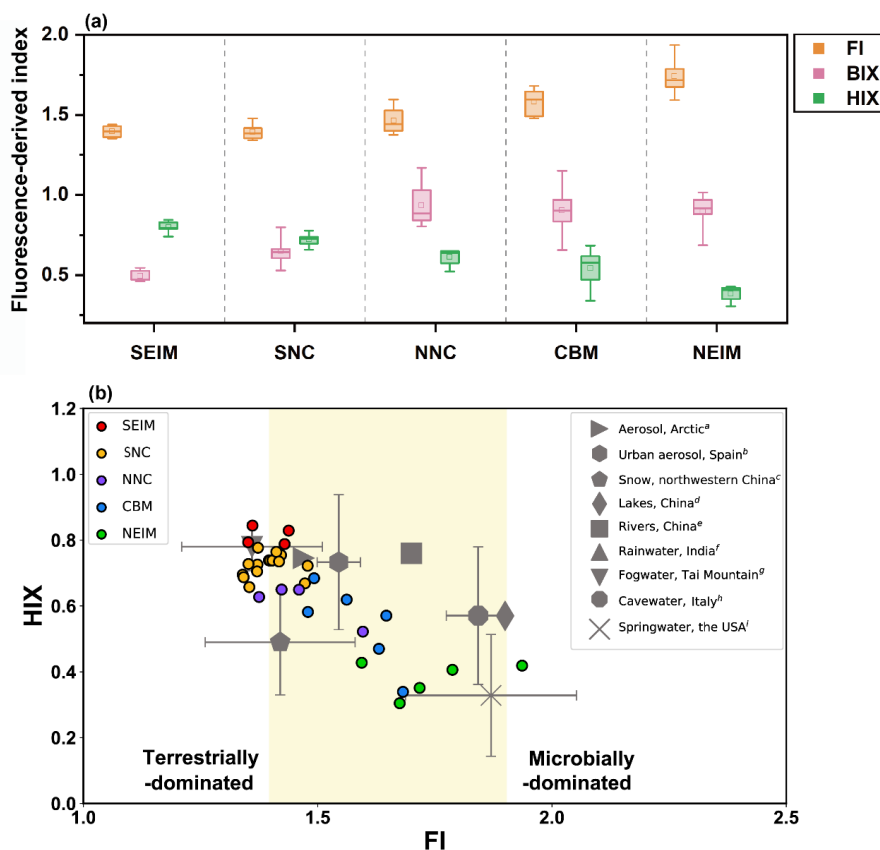
13  
 14 **Figure 3:** (a–c) Three fluorescent components identified by PARAFAC analysis. (d) Relative contributions of  
 15 the three components to total fluorescence at each site. HULIS-1, HULIS-2, and PRLIS are represented by  
 16 the specific colors shown in the legend (top left corner). The distributions of BC emissions and desert areas in  
 17 our study area are indicated by gray and light yellow, respectively, with darker gray colors indicating higher  
 18 black carbon concentrations. (e–i) Average contributions of the three components in different groups of



1 samples. BC emission data are derived from the research group at Peking University  
2 (<http://inventory.pku.edu.cn/home.html>, Wang et al., 2014a); the Chinese desert (sand) distribution dataset  
3 is provided by the National Tibetan Plateau Data Center (<http://poles.tpdc.ac.cn/zh-hans/data/122c9ac2-53ee-4b9a-ac87-1a980b131c9b/>; Wang et al., 2013a).

5 Figure 3d depicts the spatial distribution of the relative contribution of three components to fluorescence,  
6 with the regional averages given in Figure 3e–g. In SEIM, the greatest contribution is that of HULIS-1  
7 (47 %), followed by HULIS-2 (38 %) and PRLIS (15 %), indicating that the signal is dominated by local  
8 soil/dust sources, consistent with the local environment (Figs. 2 and 3d). HULIS-2 plays a greater role  
9 in SNC, where it accounts for half of the total fluorescence signals; of the remaining half, HULIS-1 is  
10 most important. This difference in key components between SEIM and SNC illustrates the change in  
11 primary source of fluorescence intensity. Indeed, with the most intensive human activity (e.g., agriculture,  
12 industrial emissions) being located in SNC (Figs. 1a and 3d; Guo and Hu, 2022), HULIS-2 might be  
13 derived from any combination of terrestrial, anthropogenic, and microbial sources. Nonetheless, in  
14 agreement with previous studies (Zhou et al., 2019b), our combined analysis suggests that anthropogenic  
15 activity is the main contributor to seasonal snow in northeastern China.

16 As in SNC, HULIS-2 also represents approximately half of the fluorescence signal in both NNC and the  
17 CBM. In the latter, which is heavily forested (Fig. 1a; Guo and Hu, 2022), the dominance of HULIS-2  
18 reflects the long-range transport of anthropogenic pollutants, as discussed in Sect. 3.1. HULIS-1 accounts  
19 for less than PRLIS in both NNC and the CBM, which we posit reflects the concealment of bare soil  
20 surfaces by deep snow and the importance of biological processes due to the heavy vegetation cover.  
21 PRLIS accounts for >50 % of the total fluorescence signal in NEIM, followed by HULIS-2; HULIS-1  
22 contributes relatively little in this region. We attribute this pattern to both the extensive grassland and  
23 forest cover, which obscures bare soil surfaces, and the distance from anthropogenic pollution, which  
24 together serve to amplify the importance of biological processes (Zhou et al., 2019a). Taken as a whole,  
25 the respective contributions of HULIS-1, HULIS-2, and PRLIS to the fluorescence signals in our study  
26 area are ~30 %, ~50 %, and ~20 %. We note that these findings correspond well with the background  
27 environmental conditions.



1  
2 Figure 4: (a) Variations in fluorescence-derived indices among the five groups. Boxes denote the 25<sup>th</sup> and 75<sup>th</sup>  
3 quantiles, and horizontal lines represent median values. Averages are shown as small boxes, the whiskers  
4 denoting maximum and minimum data. (b) Comparison plots of HIX versus FI for the seasonal snow surface  
5 samples (colored dots) from northeastern China, together with the average and standard deviation of different  
6 types of WSOC (grey markers) adapted from: Arctic aerosols (<sup>a</sup> Fu et al., 2015), Spanish urban aerosols (<sup>b</sup>  
7 Mladenov et al., 2011), seasonal snowpack in northwestern China (<sup>c</sup> Zhou et al., 2019b), Chinese lakes and  
8 rivers (<sup>d, e</sup> Zhou et al., 2017), rainwater from Rameswaram, India (<sup>f</sup> Salve et al., 2012), fog water from Tai  
9 Mountain, China (<sup>g</sup> Birdwell and Valsaraj, 2010), cave water from Frasassi Caves, Italy (<sup>h</sup> Birdwell and Engel,  
10 2010), and spring water in the USA (<sup>i</sup> Birdwell and Engel, 2010). Shaded areas represent mixed WSOC  
11 signatures.

12 The FI, BIX, and HIX indices reveal spatial variability in fluorescence characteristics and thus permit  
13 the tracing of potential sources. Regionally averaged FI, BIX, and HIX values are depicted in Figure 4a.  
14 Our results show that, in general, FI varies in the range of 1.34–1.94 (mean = 1.49), BIX between 0.46  
15 and 1.17 (mean = 0.74), and HIX between 0.30 and 0.84 (mean = 0.64). By comparison, reported mean  
16 FI, BIX, and HIX values for seasonal snow in Xinjiang (northwestern China) are 1.42, 0.76, and 0.55,



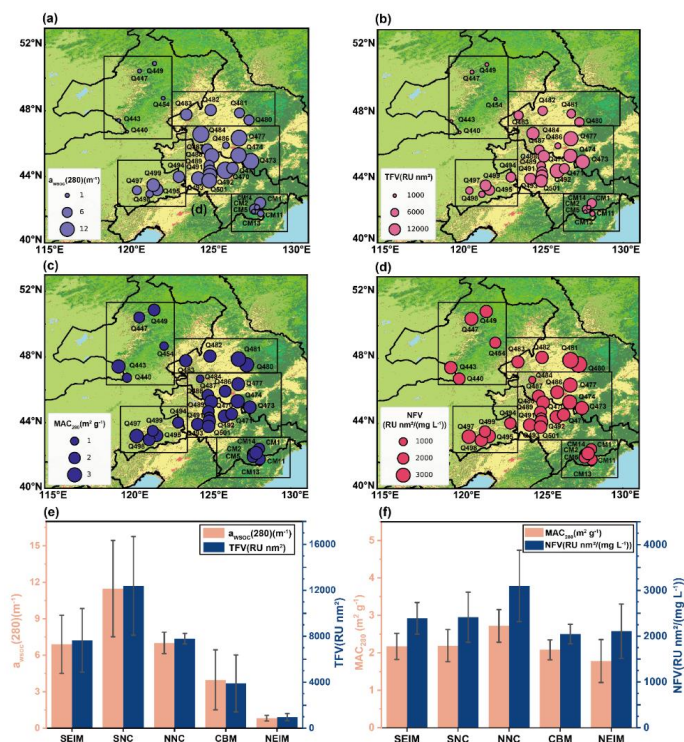
1 respectively (Zhou et al., 2019b), suggesting that the impact of humification and WSOC aromaticity are  
2 slightly higher in our study area than in Xinjiang. This outcome implies a relatively strong terrigenous  
3 signal and correspondingly weaker biogenic signal in the seasonal snowpack of northeastern China.  
4 Regionally, SEIM exhibits the lowest FI (mean = 1.40) and BIX (mean = 0.49) values but the largest  
5 HIX value (mean = 0.80), further confirming the strong influence of highly aromatic, terrestrially derived  
6 WSOC in this region relative to the others. In contrast, NEIM returns the highest FI (mean = 1.74) and  
7 BIX (mean = 0.89) values, but the lowest HIX value (mean = 0.38), indicating the dominance of low-  
8 aromatic WSOC of microbial origin. Intriguingly, our results reveal that FI and BIX rises monotonously  
9 with decreasing (increasing) fractional contributions of HULIS-1 (PRLIS), whereas HIX exhibits a  
10 similar but contrasting pattern. Together, the comprehensive dataset described above verifies the regional  
11 variability in the terrestrial contributions to WSOC, in which SEIM > SNC > NNC > CBM > NEIM; this  
12 pattern is reversed for microbially sourced WSOC.

13 Figure 4b illustrates HIX versus FI as a scatterplot, compared with published data for different sample  
14 types; the shaded area depicts the region in which the FI value is >1.4 but <1.9. As FI values of  $\leq 1.4$   
15 correspond to terrestrial sources and values of  $\geq 1.9$  denote a primarily microbial origin, values of 1.4–  
16 1.9 suggest a mixed origin. In general, FI exhibits a rising trend with declining HIX across northeastern  
17 China. For both SEIM and SNC, FI occupies a narrow range centered on 1.4, indicating either a  
18 predominantly terrestrial or mixed origin. We note that these results are comparable to those of fog water  
19 from the Tai Mountain, Arctic atmospheric aerosols, and seasonal snow in northwestern China (Birdwell  
20 and Valsaraj, 2010; Fu et al., 2015; Zhou et al., 2019b). Further, we highlight that HIX values are  
21 marginally higher in SEIM than elsewhere, suggesting a stronger influence from highly humified WSOC  
22 that probably reflects the extensive deserts and exposed earth in this region. FI values for NNC and the  
23 CBM fall within the range of 1.4–1.7 and thus reflect a mixed origin, in line with previous data from  
24 urban aerosols in Spain and Chinese river water samples (Mladenov et al., 2011, Zhou et al., 2017).  
25 When combined, FI and HIX values for NNC and CBM snowpack indicate that WSOC in these regions  
26 bears a stronger terrestrial signature than do water samples from Chinese lakes and Italian caves  
27 (Birdwell and Engel, 2010; Zhou et al., 2017). Finally, FI values for NEIM fall within a range of 1.6–  
28 2.0, comparable to values from spring water in the USA (Birdwell and Engel, 2010), thus implying a  
29 predominantly microbial or mixed origin.



### 1 3.3 Comparisons of fluorescence and absorption characteristics

2 Figure 5a depicts TFV as a measure of the spatial distribution of absolute WSOC fluorescence intensity  
 3 in the snowpack of northeastern China;  $a_{\text{WSOC}}(280)$  is shown in Figure 5b for comparison. In general,  
 4 TFV and  $a_{\text{WSOC}}(280)$  both exhibit large spatial variability in the range of 690–18600  $\text{RU}\cdot\text{nm}^2$  and 0.42–  
 5  $16.98\text{ m}^{-1}$ , respectively. Regional mean values are  $7700 \pm 2800\text{ RU}\cdot\text{nm}^2$  (TFV) and  $6.90 \pm 2.39\text{ m}^{-1}$   
 6 ( $a_{\text{WSOC}}(280)$ ) for SEIM,  $12400 \pm 4300\text{ RU}\cdot\text{nm}^2$  (TFV) and  $11.48 \pm 3.96\text{ m}^{-1}$  ( $a_{\text{WSOC}}(280)$ ) for SNC,  $7800$   
 7  $\pm 500\text{ RU}\cdot\text{nm}^2$  (TFV) and  $7.02 \pm 0.88\text{ m}^{-1}$  ( $a_{\text{WSOC}}(280)$ ) for NNC,  $3900 \pm 2500\text{ RU}\cdot\text{nm}^2$  (TFV) and  $3.97$   
 8  $\pm 2.46\text{ m}^{-1}$  ( $a_{\text{WSOC}}(280)$ ) for the CBM, and  $1000 \pm 300\text{ RU}\cdot\text{nm}^2$  (TFV) and  $0.83 \pm 0.23\text{ m}^{-1}$  ( $a_{\text{WSOC}}(280)$ )  
 9 for NEIM. We note that both distributions are consistent in space (Fig. 5e), with the highest  
 10 concentrations in SNC and the lowest in NEIM. Moreover, the  $a_{\text{WSOC}}(280)$  value for SNC is an order of  
 11 magnitude larger than that for NEIM, implying that the impact of WSOC on snow albedo at UV  
 12 wavelengths is significant in SNC but less notable in NEIM in general (see Sect. 3.5). Previous work has  
 13 reported a similarly broad range of snowpack  $a_{\text{WSOC}}(280)$  ( $0.15\text{--}10.57\text{ m}^{-1}$ ) in northwestern China (Zhou  
 14 et al., 2019b).





1 **Figure 5: Spatial distribution of (a)  $awsoc(280)$  ( $m^{-1}$ ), (b)  $MAC_{280}$ , ( $m^2 g^{-1}$ ), (c) TFV ( $RU nm^2$ ), and (d) NFV**  
2 **( $RU nm^2 (mg L^{-1})^{-1}$ ). Regional averages for (e)  $awsoc(280)$ , TFV, (f)  $MAC_{280}$  and NFV for the five groups.**  
3 **Error bars in (e) and (f) represent the standard deviations of  $awsoc(280)$ ,  $MAC_{280}$ , TFV, and NFV for the five**  
4 **groups, respectively.**

5 Two additional fluorescence and absorption capacity indices, identified as NFV and  $MAC_{280}$ , are proven  
6 tools for revealing WSOC's fluorescence and absorption characteristics and they are related to chemical  
7 composition, structure, and source (Chen et al., 2019a). For our study area as a whole, mean NFV and  
8  $MAC_{280}$  values are  $2411.57 \pm 373.63 RU nm^2 (mg L^{-1})^{-1}$  and  $2.17 \pm 0.49 m^2 g^{-1}$ , respectively. Both  
9 indices exhibit a narrow range, with regional means ranging from  $2100 \pm 600$  to  $3100 \pm 800 RU nm^2$   
10  $(mg L^{-1})^{-1}$  and from  $1.78 \pm 0.57$  to  $2.72 \pm 0.44 m^2 g^{-1}$ , respectively, in contrast to the broad inter-regional  
11 disparities in TFV and  $awsoc(280)$ . Moreover, the spatial patterns of NFV and  $MAC_{280}$  are similar, with  
12 the highest values in NNC. We speculate that this result reflects the comparatively high low-oxygenated  
13 HULIS-2 fraction measured in the NNC samples (Fig. 3g), as the lower-oxygenated BrC (e.g., HULIS-  
14 2) has a higher absorption capacity (Browne et al., 2019).

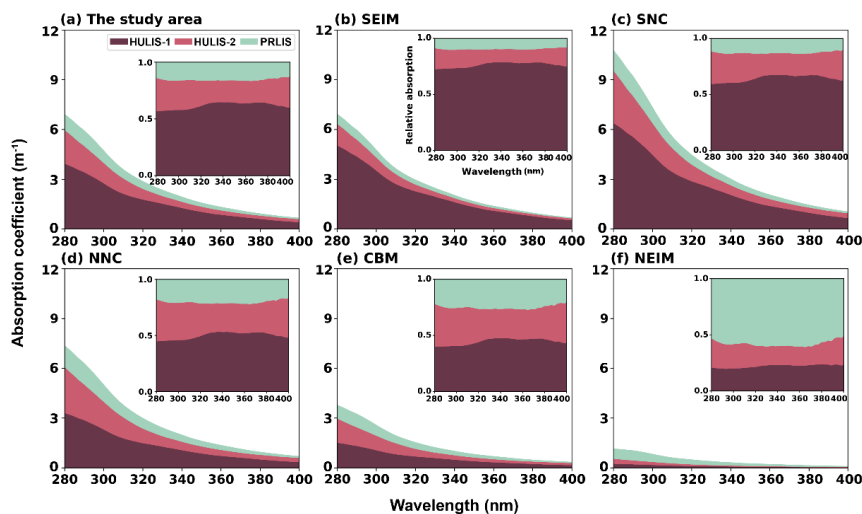
15 Scatterplots for  $awsoc(280)$  with TFV,  $F_{max}(HULIS-1)$ ,  $F_{max}(HULIS-2)$ , and  $F_{max}(PRLIS)$  are provided in  
16 Figure S4 to further demonstrate the close relationship between fluorescence and the absorption  
17 characteristics of WSOC in our snow samples. As samples Q480, Q484, and Q477 deviate considerably  
18 from the respective confidence intervals, we did not include them in our analyses. Surprisingly, we found  
19 that TFV is closely correlated to  $awsoc(280)$ , with  $P < 0.001$  and all datapoints located close to the line  
20 of best fit, indicating that the three components (HULIS-1, HULIS-2, PRLIS) contributing to the total  
21 fluorescence are also responsible for the majority of absorption. For each component, our data show that  
22  $F_{max}(HULIS-1)$  is most closely correlated with  $awsoc(280)$ , followed by  $F_{max}(HULIS-2)$ . The correlation  
23 between  $F_{max}(PRLIS)$  and  $awsoc(280)$  is the poorest, yet it is still significant ( $P < 0.001$ ). Together, our  
24 results imply that HULIS-1 is probably the greatest contributor to light absorption, with PRLIS being the  
25 least important.

### 26 **3.4 Fractional contributions of different WSOC components to light absorption**

27 Previous studies of atmospheric aerosols, water, and snow/glacier ice have typically regarded WSOC as  
28 a whole when discussing its impact on light absorption (Barrett and Sheesley, 2017; D'Sa et al., 2014;  
29 Niu et al., 2018; Wu et al., 2019). Yet, depending on environmental conditions, the various components  
30 of WSOC play measurably different roles in light absorption according to their concentrations and optical



1 properties (Zhou et al., 2022). Although the qualitative analysis described above have provided plausible  
2 information about the component-specific influence of WSOC on light absorption, the quantitative  
3 fractional contributions of specific components to light absorption are still unknown. Recently, Chen et  
4 al. (2019a) collected atmospheric aerosol samples in PM<sub>2.5</sub> over Xi'an, China, and successfully attributed  
5 the dithiothreitol (DTT) activity levels to various BrC components by coupling DDT and BrC datasets.  
6 A similar attribution method has been applied to various research areas, including climate change,  
7 extreme weather, and atmospheric environments (Cao et al., 2015; Pokrovsky, 2019; Xin et al., 2016;  
8 Zhao et al., 2019). In this study, we applied a multiple linear regression method comparable to that of  
9 Chen et al. (2019a) to derive the fractional contribution of each WSOC component to light absorption.  
10 We note that, despite this method having been used elsewhere (Wu et al., 2022; Wu et al., 2021), it  
11 remains a highly innovative approach to evaluating the light absorption of snowpack WSOC.  
12 Table S3 lists the statistical results of the fitted light absorption coefficient, based on the F<sub>max</sub> data for  
13 three fluorescent components of EEM analysis. As the fitted results can explain ~94 %–99 % of the  
14 variance in measured light absorption within the 280–400 nm range, we conclude that the fusion of  
15 multiple fluorescent components is an effective means of describing most of the spatial features of  
16 WSOC light absorption throughout northeastern China. Accordingly, the wavelength-dependent  
17 fractional contributions of each component of light absorption in this band (280–400 nm) are reported in  
18 Figure 6. For our entire study area, light absorption is dominated by high-oxygenated HULIS-1, which  
19 accounts for ~56 %–65 % of the contribution across UV wavelengths. Further, we observed that the  
20 HULIS-1 contribution rises slightly from 280 to ~340 nm, after which there is a decreasing trend as  
21 wavelength increases. In contrast, HULIS-2 exhibits a valley-type pattern in fractional contribution  
22 between 280 and 400 nm and is responsible for ~19 %–30 % of all light absorption.



1

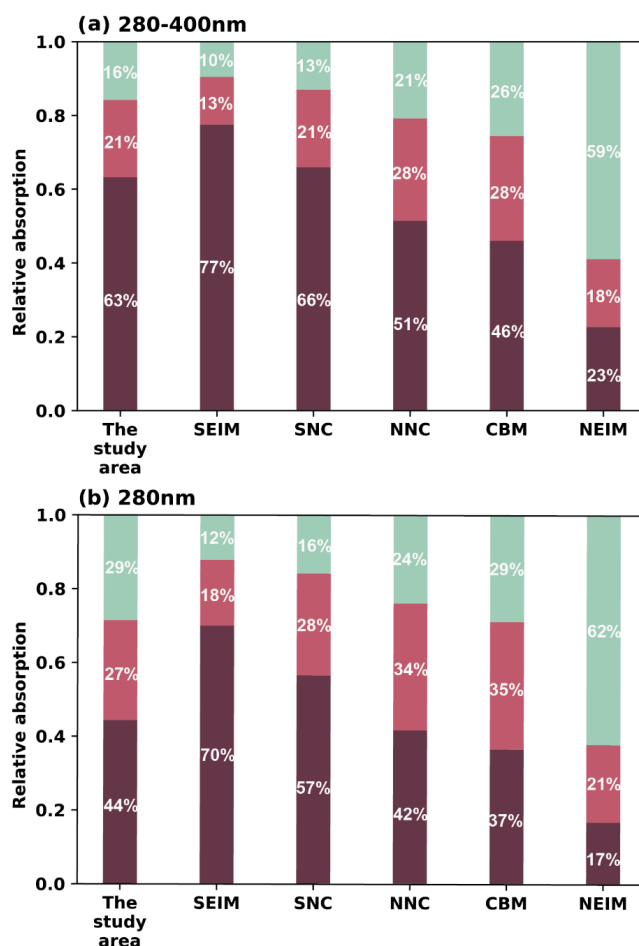
2 **Figure 6:** Relative contributions of the three components to the total absorption of samples in (a) the whole  
3 study area and (b–f) each of the five groups.

4 PRLIS contributes the least (~12 %–17 %) to light absorption and exhibits a similar wavelength-  
5 dependent pattern to HULIS-1. These results are consistent with the qualitatively comparative analysis  
6 described in Sect. 3.3. Previous studies have also highlighted this dominance of high-oxygenated  
7 compounds in WSOC light absorption, based on samples impacted by naturally and anthropogenically  
8 derived soils (Zhou et al., 2022). Conversely, the total absorption coefficient of WSOC decreases with  
9 increasing wavelength between 280 and 400 nm, in accord with previous studies (Andreae and Gelencser,  
10 2006; Chakrabarty et al., 2010; Gustafsson et al., 2009; Wu et al., 2019). The AAE lies primarily between  
11 5.0 and 8.0 (mean = 6.6) in the range of 280–400 nm, which is in agreement with results from snow  
12 collected from the Arctic, the northern Tibetan Plateau, and northwestern China (Voisin et al., 2012; Yan  
13 et al., 2016; Zhou et al., 2021).

14 For each component, the wavelength-dependent variability in light absorption is similar among all five  
15 regions, although the magnitude of each contribution varies from region to region. Moreover, compared  
16 with the spectral results, we found that the solar-radiation-weighted broadband light absorption was a  
17 more meaningful parameter for researchers studying climate change and atmospheric radiation.  
18 Therefore, the broadband results in Figure 7a for 280–400 nm absorption contributions—HULIS-1  
19 (62 %), HULIS-2 (21 %), and PRLIS (17 %)—are average values for the whole study area. On a regional  
20 scale, the HULIS-1 contribution to light absorption (280–400 nm) follows the spatial pattern SEIM >



1 SNC > NNC > CBM > NEIM. We note that HULIS-1 dominates light absorption in SEIM, SNC, and  
2 NNC but has a minor impact in NEIM compared with the other two components. In contrast, the impact  
3 of HULIS-2 varies only slightly among the five regions, with the greatest contributions in NNC and  
4 CMB, and the lowest in NEIM. The contribution of PRLIS is essentially opposite that of HULIS-1, being  
5 dominant in NEIM but of relatively minor important elsewhere. As shown in Figure 7b, light absorption  
6 contributions at 280 nm are consistent with the broadband results (Fig. 7a) in terms of the regional pattern,  
7 although specific values differ because of the different wavelength-dependent properties of light  
8 absorption for the three WSOC components.



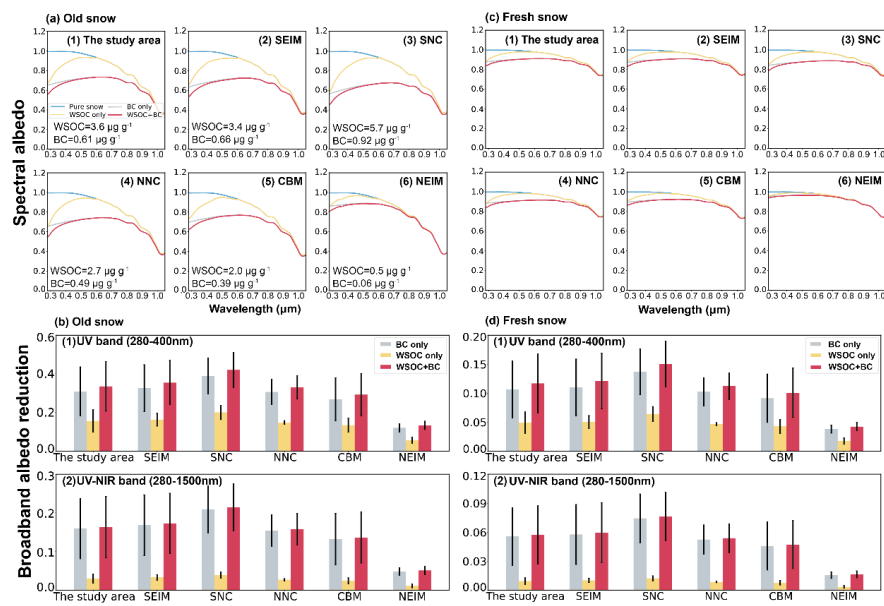
9  
10 Figure 7: Regional averages for the relative contributions of the three fluorescent components to light  
11 absorption at wavelengths of (a) 280 nm and (b) 280–400 nm.



1 We find it noteworthy that, for each component, the overall regional pattern of its contribution to light  
2 absorption aligns with its impact on fluorescence signals, thereby confirming the viability of the  
3 attribution analysis employed in our study. Nonetheless, we observed that the magnitude of each  
4 component's contribution varies relative to its respective fluorescence signal. For instance, HULIS-1  
5 returns a greater contribution to light absorption than its fluorescence signal, in contrast to HULIS-2.  
6 One plausible explanation for this discrepancy is that the fluorescence quantum yields (AQYs), which  
7 are essentially the ratio of fluorescence intensity versus absorption intensity, are different for each  
8 component. Indeed, in their comprehensive field-based study of BrC fluorescence and absorption  
9 properties in northern China, Wen et al. (2021) reported that the AQYs of WSOC decrease with  
10 increasing HIX, meaning that components with higher HIX values, such as HULIS-1, have lower AQYs  
11 than does HULIS-2. Thus, the contribution of HULIS-1 to the fluorescence signals will be smaller than  
12 its contribution to light absorption, and vice versa for HULIS-2.

### 13 **3.5 Albedo reduction and radiative forcing attributed to snowpack WSOC**

14 The strong light absorption of WSOC in UV bands has important ramifications for snow albedo and  
15 radiative forcing throughout northeastern China. However, owing to the chemical and optical complexity  
16 of WSOC components, quantitative estimates for snowpack light absorption remain poorly understood.  
17 For example, although prior work in northeastern China has focused on BC (Wang et al., 2013b) and  
18 other water-insoluble light-absorbing particles (Wang et al., 2017; Zhao et al., 2014) via field  
19 measurements, model simulations, and satellite remote sensing (Pu et al., 2019), the specific impacts of  
20 WSOC have not been studied. Consequently, ours is the first study to report on the impact of WSOC on  
21 snow albedo and radiative forcing in northeastern China and to compare these data with BC results to  
22 highlight the non-negligible role of WSOC.



1

2 **Figure 8: (a) and (b): Simulated snow spectral albedo and broadband albedo reductions—under various**  
3 **contamination scenarios and for different regions—for old snow (radius = 1000  $\mu\text{m}$ ). (c), (d) Simulated snow**  
4 **spectral albedo and broadband albedo reductions—under various contamination scenarios and for different**  
5 **regions—for fresh snow (radius = 100  $\mu\text{m}$ ). Colors represent the different types of snow (pure snow, BC- or**  
6 **WSOC-contaminated snow, and snow polluted by both WSOC and BC).**

7

8 Figure 8 shows the regional-mean spectral snow albedo as well as the reduction in albedo due to WSOC,  
9 BC, and WSOC + BC. We assume a snow radius of 100  $\mu\text{m}$  for fresh snow and 1000  $\mu\text{m}$  for old snow.

10

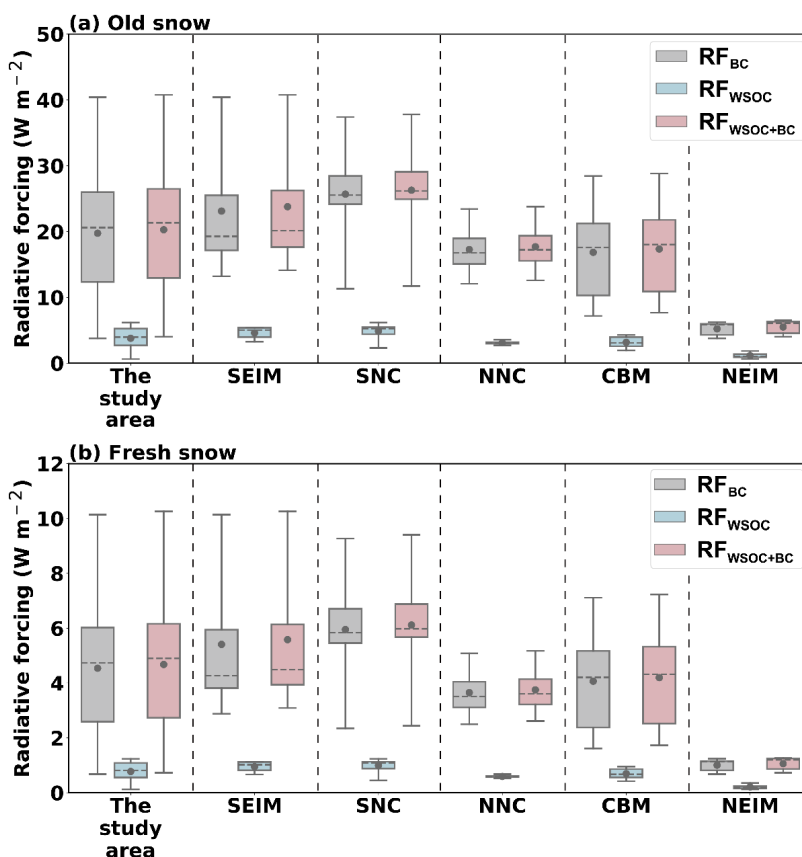
11 Our findings reveal that WSOC induces a marked decline in albedo within the UV and short-wave VIS  
12 bands, with the magnitude of albedo reduction growing rapidly as wavelength shrinks owing to the large  
13 AAE value of WSOC. In comparison, BC induces a widespread albedo reduction spanning the UV to  
14 NIR bands, and wavelength-dependent variations are significantly smaller than those of WSOC. For VIS  
15 and NIR, the reduction in albedo is dominated by BC, whereas the impacts of WSOC and BC are  
16 comparable in UV wavelengths, a pattern that is consistent with the results of studies of atmospheric  
17 aerosols (Shamjad et al., 2016). We note that these characteristics persist throughout northeastern China  
18 despite regional variability in environmental conditions and snowpack types (old vs. fresh snow).

17

18 For broadband wavelengths, our results indicate that the WSOC-induced (mean = 3.6  $\mu\text{g g}^{-1}$ ) albedo  
19 reduction for 280–400 nm wavelengths in old (fresh) snow is 0.16 (0.05) across the whole study area,  
20 which corresponds to approximately 50.3 % (46.3 %) the impact of BC (mean = 0.6  $\mu\text{g g}^{-1}$ ). Regionally,



1 the greatest decline in albedo occurred in SNC, where a mean WSOC of  $5.7 \mu\text{g g}^{-1}$  resulted in a reduction  
2 of 0.20 (0.06) in the 280–400 nm range for old (fresh) snow. In contrast, the smallest decline in albedo  
3 was observed in NEIM, with reductions of 0.06 (0.02) resulting from an average WSOC concentration  
4 of  $0.5 \mu\text{g g}^{-1}$ . Compared with the UV bands, a WSOC-induced albedo reduction of 0.03 (0.009) over the  
5 UV–NIR range (280–1500 nm) accounts for only ~18.8 % (16.7 %) of that due to BC in our study area.  
6 The regional mean for old (fresh) snow falls in the range of 0.01–0.04 (0.003–0.012), with the highest  
7 (lowest) values occurring in SNC (NEIM). However, we observed the highest ratio of WSOC- to BC-  
8 induced albedo reduction in NEIM. Together, these results indicate that WSOC plays a potentially  
9 important role in altering UV snow albedo in NEIM, despite its relatively low concentrations in the  
10 regional snowpack.



11  
12 Figure 9: Radiative forcing due to different pollutants in (a) old or (b) fresh snow. Gray, blue, and red indicate  
13 the radiative forcing of BC, WSOC, and BC + WSOC, respectively.



1 Radiative forcing is an important index that directly reflects the impact of snowpack WSOC on the  
2 regional radiation balance and climate (Beres et al., 2020). Previous studies have tended to focus on  
3 calculating instantaneous radiative forcing values; however, in reality, time-averaged results are more  
4 valuable for climate research. Here, we present data on the daily mean radiative forcing due to WSOC,  
5 BC, and WSCO + BC (Fig. 9), calculated using the methodology of Wang et al. (2017). In general, for  
6 northeastern China we found the mean radiative forcing of WSOC in old (fresh) snow to be 3.78 (0.77)  
7  $\text{W m}^{-2}$ , with regional mean values varying from 1.15 (0.21) to 4.88 (1.0)  $\text{W m}^{-2}$ . Zhou et al. (2021)  
8 reported daily mean radiative forcing by regional WSOC (0.6–7.1  $\mu\text{g g}^{-1}$ ) of between  $\sim 0.04$  and  $\sim 0.59$   
9  $\text{W m}^{-2}$  for northwestern China, which is comparable to our values in fresh snow. Furthermore, the ratio  
10 of WSOC-driven to BC-driven radiative forcing varies within the range of 10.3 %–32.0 % (9.8 %–30.8 %)  
11 for old (fresh) snow, which is consistent with the results of our calculated albedo reductions. These results  
12 confirm that the role of WSOC must not be ignored in discussions about radiative balance in northeastern  
13 China. Similarly, the sizeable impact of WSOC on the absorption of UV radiation has the potential to  
14 influence biogeochemistry (Helms et al., 2013; Seekell et al., 2015) and snow photochemical processes  
15 (e.g., photolysis of nitrate ( $\text{NO}_3^-$ ) and nitrite ( $\text{NO}_2^-$ ) in snow, in addition to the release of  $\text{NO}_x$  ( $\text{NO} +$   
16  $\text{NO}_2$  and HONO). Snow photochemistry is beyond the scope of this study, however, the high  
17 concentrations of WSOC and nitrate (not shown) pollution in northeastern China make this a logical next  
18 step for research in this field.

#### 19 **4 Conclusions and atmospheric implications**

20 During 2020 and 2021, we collected 34 surface samples of seasonal snow from sites throughout  
21 northeastern China to investigate the fluorescence characteristics, optical properties, and radiative effects  
22 of snowpack WSOC. With an average concentration of WSOC of  $3.59 \pm 3.19 \mu\text{g g}^{-1}$ , our results returned  
23 regional mean values of  $3.35 \pm 1.49 \mu\text{g g}^{-1}$  (SEIM),  $5.73 \pm 3.68 \mu\text{g g}^{-1}$  (SNC),  $2.70 \pm 0.75 \mu\text{g g}^{-1}$  (NNC),  
24  $1.95 \pm 1.28 \mu\text{g g}^{-1}$  (CBM), and  $0.50 \pm 0.19 \mu\text{g g}^{-1}$  (NEIM), indicating a considerable degree of regional  
25 variability of WSOC mass loadings. Measured values of WSOC fluorescence intensity (690–18600 RU  
26  $\text{nm}^2$ ) and light absorption (0.4–17.0  $\text{m}^{-1}$ ) are also highly variable.  
27 In the first study of its kind, we used EEMs and PARAFAC to identify three fluorescence WSOC  
28 components prevalent in northeastern China. Specifically, these include the high-oxygenated HULIS-1,



1 which is a terrigenous, humic-like component, and the low-oxygenated HULIS-2, which is a humic-like  
2 component derived from mixed sources, such as anthropogenic activity, microbial processes, and soil.  
3 The third component, PRLIS, is a protein-like substance derived from autochthonous biological activity.  
4 In SEIM, which is characterized by desert and bare soil surfaces, the HULIS-1 signal is dominant (47 %) and the HIX value is the highest, whereas FI and BIX are the lowest. Together, these findings reveal a  
5 high degree of humification and minimal bioavailability, indicating that snowpack WSOC originates  
6 primarily from soil sources. In contrast, the PRLIS signal (58 %) dominates in NEIM, which also exhibits  
7 the lowest HIX values and highest FI and BIX values. We propose that the elevated bioavailability of  
8 this remote, forested region indicates a predominantly biological origin for NEIM snowpack WSOC.  
9 HULIS-2 dominates the densely populated and intensively farmed SNC (51 %) and NNC (57 %) regions,  
10 where HIX, FI, and BIX values are moderate, leading us to conclude that snowpack WSOC is of mixed  
11 origin.  
12  
13 We employed multiple regression analysis to estimate the fractional contributions of different WSOC  
14 components to snowpack light absorption. Throughout our study area, HULIS-1 tends to be the greatest  
15 contributor (~56 %–65 %) over the 280–400 nm range, followed by HULIS-2 (~19 %–30 %) and PRLIS  
16 (~12 %–17 %). On a more regional basis, light absorption remains dominated by HULIS-1 in SEIM,  
17 SNC, NNC, and the CBM, whereas PRLIS takes a leading role in NEIM. In contrast to its primary role  
18 in fluorescence, the contribution of HULIS-2 to light absorption is relatively low across all regions,  
19 potentially reflecting the variable fluorescence quantum yields (AQYs) of the different components.  
20 Finally, we compared the impact on snow albedo and radiative forcing of WSOC relative to BC. With  
21 an average concentration of  $3.6 \mu\text{g g}^{-1}$ , our results indicate that WSOC induces an albedo reduction  
22 across northeastern China of 0.16 (0.05) in old (fresh) snow over the 280–400 nm range, and thus  
23 represents approximately 50 % (46 %) of the albedo reduction due to BC (average concentration =  $0.6 \mu\text{g g}^{-1}$ ). We note, however, that the WSOC-driven reduction in the UV–NIR spectrum (280–1500 nm) is  
24 only 0.03 (0.009), corresponding to 19 % (17 %) that of BC. The average radiative forcing of WSOC in  
25 old (fresh) snow in northeastern China is  $3.8 (0.8) \text{ W m}^{-2}$ , equating to 19 % (17 %) of the BC-induced  
26 radiative forcing.  
27  
28 We indicate that our study could contribute to the understanding of carbon cycling processes, regional  
29 air quality, hydrological processes, and climate change in the earth systems. For example, the abundant



1 WSCO concentrations measured in this study implied the significant carbon input from the  
2 atmosphere to the snowpack through wet or dry depositions in northeastern China. While the complex  
3 chemical compositions of snowpack WSOC could further influence the carbon balance of the snow  
4 environment by affecting microbial activities (Stedmon et al., 2007). The strong absorption properties of  
5 WSOC in the UV-Vis band also implied its important role in initiating snow photochemistry (McNeill  
6 et al., 2012), which will change the composition of organic compounds in the snow in turn (Grannas et  
7 al., 2007), and affect the surrounding air quality by releasing oxidizing gas like NO<sub>x</sub> into the atmosphere  
8 (Zatko et al., 2013). Moreover, the non-negligible influence of WSOC on the snow albedo and radiative  
9 effect indicated that it could not only accelerate snow melting, change the periods and mass of water and  
10 carbon exchange between snowpack and underlying soils or vegetation (Meyer and Wania, 2008) , but  
11 also potentially affect regional climate through changing the surface radiative balance (Beres et al., 2020) .

12 *Data availability.* Data presented and used throughout this study can be accessed through the  
13 following data repository: <https://doi.org/10.5281/zenodo.6541956>.

14 *Supplement.* The supplement related to this article is available online at:

15 *Author contributions.* XN and WP designed the study and wrote the first draft with contributions  
16 from all coauthors. XN designed and conducted the lab experiments with the assistance of YZ and  
17 HW. XN processed the data with the assistance of DW and TS. XN, WP, YC, YX, TS designed  
18 and conducted the field campaign. XW supervised this study. All co-authors commented on the  
19 paper and improved it.

20 *Competing interests.* The authors declare that they have no conflict of interest.



1 *Acknowledgements.* The Lanzhou University group acknowledges support from the National  
2 Science Fund for Distinguished Young Scholars and the National Natural Science Foundation of  
3 China.  
4 *Financial support.* This research was supported by the National Science Fund for Distinguished  
5 Young Scholars (42025102), the National Natural Science Foundation of China (42075061 and  
6 41975157), and the Lanzhou City's scientific research funding subsidy to Lanzhou University.

#### 7 **References**

- 8 Anastasio, C. and Robles, T.: Light absorption by soluble chemical species in Arctic and Antarctic snow,  
9 J. Geophys. Res., 112, D24304, <https://doi.org/10/dt7c54>, 2007.
- 10 Andreae, M. O. and Gelencser, A.: Black carbon or brown carbon? The nature of light-absorbing  
11 carbonaceous aerosols, 18, <https://doi.org/10/fd772v>, 2006.
- 12 Antony, R., Grannas, A. M., Willoughby, A. S., Sleighter, R. L., Thamban, M., and Hatcher, P. G.: Origin  
13 and Sources of Dissolved Organic Matter in Snow on the East Antarctic Ice Sheet, Environ. Sci.  
14 Technol., 48, 6151–6159, <https://doi.org/10.1021/es405246a>, 2014.
- 15 Bahram, M., Bro, R., Stedmon, C., and Afkhami, A.: Handling of Rayleigh and Raman scatter for  
16 PARAFAC modeling of fluorescence data using interpolation, 20, 99–105,  
17 <https://doi.org/10.1002/cem.978>, 2006.
- 18 Barnett, T. P., Pierce, D. W., Hidalgo, H. G., Bonfils, C., Santer, B. D., Das, T., Bala, G., Wood, A. W.,  
19 Nozawa, T., Mirin, A. A., Cayan, D. R., and Dettinger, M. D.: Human-Induced Changes in the  
20 Hydrology of the Western United States, Science, 319, 1080–1083,  
21 <https://doi.org/10.1126/science.1152538>, 2008.
- 22 Barrett, T. E. and Sheesley, R. J.: Year-round optical properties and source characterization of Arctic  
23 organic carbon aerosols on the North Slope Alaska, 122, 9319–9331,  
24 <https://doi.org/10.1002/2016JD026194>, 2017.
- 25 Battin, T. J., Luyssaert, S., Kaplan, L. A., Aufdenkampe, A. K., Richter, A., and Tranvik, L. J.: The  
26 boundless carbon cycle, Nature Geosci, 2, 598–600, <https://doi.org/10.1038/ngeo618>, 2009.



- 1 Beine, H., Anastasio, C., Esposito, G., Patten, K., Wilkening, E., Domine, F., Voisin, D., Barret, M.,  
2 Houdier, S., and Hall, S.: Soluble, light-absorbing species in snow at Barrow, Alaska, *J. Geophys. Res.*,  
3 116, D00R05, <https://doi.org/10.1029/2011JD016181>, 2011.
- 4 Beniston, M., Farinotti, D., Stoffel, M., Andreassen, L. M., Coppola, E., Eckert, N., Fantini, A., Giacona,  
5 F., Hauck, C., Huss, M., Huwald, H., Lehning, M., López-Moreno, J.-I., Magnusson, J., Marty, C.,  
6 Moran-Tejeda, E., Morin, S., Naaim, M., Provenzale, A., Rabatel, A., Six, D., Stötter, J., Strasser, U.,  
7 Terzago, S., and Vincent, C.: The European mountain cryosphere: A review of past, current and future  
8 issues, *Alpine Glaciers*, <https://doi.org/10.5194/tc-2016-290>, 2017.
- 9 Beres, N. D., Sengupta, D., Samburova, V., Khlystov, A. Y., and Moosmüller, H.: Deposition of brown  
10 carbon onto snow: changes in snow optical and radiative properties, *Atmos. Chem. Phys.*, 20, 6095–  
11 6114, <https://doi.org/10.5194/acp-20-6095-2020>, 2020.
- 12 Birdwell, J. E. and Engel, A. S.: Characterization of dissolved organic matter in cave and spring waters  
13 using UV–Vis absorbance and fluorescence spectroscopy, *Organic Geochemistry*, 41, 270–280,  
14 <https://doi.org/10.1016/j.orggeochem.2009.11.002>, 2010.
- 15 Birdwell, J. E. and Valsaraj, K. T.: Characterization of dissolved organic matter in fogwater by excitation–  
16 emission matrix fluorescence spectroscopy, *Atmospheric Environment*, 44, 3246–3253,  
17 <https://doi.org/10.1016/j.atmosenv.2010.05.055>, 2010.
- 18 Bond, T. C., Doherty, S. J., Fahey, D. W., Forster, P. M., Berntsen, T., DeAngelo, B. J., Flanner, M. G.,  
19 Ghan, S., Kärcher, B., Koch, D., Kinne, S., Kondo, Y., Quinn, P. K., Sarofim, M. C., Schultz, M. G.,  
20 Schulz, M., Venkataraman, C., Zhang, H., Zhang, S., Bellouin, N., Guttikunda, S. K., Hopke, P. K.,  
21 Jacobson, M. Z., Kaiser, J. W., Klimont, Z., Lohmann, U., Schwarz, J. P., Shindell, D., Storelvmo, T.,  
22 Warren, S. G., and Zender, C. S.: Bounding the role of black carbon in the climate system: A scientific  
23 assessment, 118, 5380–5552, <https://doi.org/10.1002/jgrd.50171>, 2013.
- 24 Browne, E. C., Zhang, X., Franklin, J. P., Ridley, K. J., Kirchstetter, T. W., Wilson, K. R., Cappa, C. D.,  
25 and Kroll, J. H.: Effect of heterogeneous oxidative aging on light absorption by biomass burning  
26 organic aerosol, *Aerosol Science and Technology*, 53, 663–674,  
27 <https://doi.org/10.1080/02786826.2019.1599321>, 2019.
- 28 Cao, L., Bala, G., Zheng, M., and Caldeira, K.: Fast and slow climate responses to CO<sub>2</sub> and solar forcing:  
29 A linear multivariate regression model characterizing transient climate change, 120, 12,037–12,053,



- 1 <https://doi.org/10.1002/2015JD023901>, 2015.
- 2 Chakrabarty, R. K., Moosmüller, H., Chen, L.-W. A., Lewis, K., Arnott, W. P., Mazzoleni, C., Dubey, M.  
3 K., Wold, C. E., Hao, W. M., and Kreidenweis, S. M.: Brown carbon in tar balls from smoldering  
4 biomass combustion, *Atmos. Chem. Phys.*, 10, 6363–6370, <https://doi.org/10.5194/acp-10-6363-2010>,  
5 2010.
- 6 Chen, Q., Miyazaki, Y., Kawamura, K., Matsumoto, K., Coburn, S., Volkamer, R., Iwamoto, Y., Kagami,  
7 S., Deng, Y., Ogawa, S., Ramasamy, S., Kato, S., Ida, A., Kajii, Y., and Mochida, M.: Characterization  
8 of Chromophoric Water-Soluble Organic Matter in Urban, Forest, and Marine Aerosols by HR-ToF-  
9 AMS Analysis and Excitation–Emission Matrix Spectroscopy, *Environ. Sci. Technol.*, 50, 10351–  
10 10360, <https://doi.org/10.1021/acs.est.6b01643>, 2016.
- 11 Chen, Q., Wang, M., Wang, Y., Zhang, L., Li, Y., and Han, Y.: Oxidative Potential of Water-Soluble  
12 Matter Associated with Chromophoric Substances in PM<sub>2.5</sub> over Xi’an, China, *Environ. Sci. Technol.*,  
13 53, 8574–8584, <https://doi.org/10.1021/acs.est.9b01976>, 2019a.
- 14 Chen, Q., Mu, Z., Song, W., Wang, Y., Yang, Z., Zhang, L., and Zhang, Y.: Size-Resolved  
15 Characterization of the Chromophores in Atmospheric Particulate Matter From a Typical Coal-  
16 Burning City in China, *J. Geophys. Res. Atmos.*, 124, 10546–10563,  
17 <https://doi.org/10.1029/2019JD031149>, 2019b.
- 18 Choi, Y., Kanaya, Y., Park, S.-M., Matsuki, A., Sadanaga, Y., Kim, S.-W., Uno, I., Pan, X., Lee, M., Kim,  
19 H., and Jung, D. H.: Regional variability in black carbon and carbon monoxide ratio from long-term  
20 observations over East Asia: assessment of representativeness for black carbon (BC) and carbon  
21 monoxide (CO) emission inventories, *Atmos. Chem. Phys.*, 20, 83–98, <https://doi.org/10.5194/acp-20-83-2020>, 2020.
- 23 Coble, P. G.: Characterization of marine and terrestrial DOM in seawater using excitation-emission  
24 matrix spectroscopy, *Marine Chemistry*, 51, 325–346, [https://doi.org/10.1016/0304-4203\(95\)00062-3](https://doi.org/10.1016/0304-4203(95)00062-3),  
25 1996.
- 26 Coble, P. G., Green, S. A., Blough, N. V., and Gagosian, R. B.: Characterization of dissolved organic  
27 matter in the Black Sea by fluorescence spectroscopy, *Nature*, 348, 432–435,  
28 <https://doi.org/10.1038/348432a0>, 1990.
- 29 Coble, P. G., Del Castillo, C. E., and Avril, B.: Distribution and optical properties of CDOM in the



- 1 Arabian Sea during the 1995 Southwest Monsoon, *Deep Sea Research Part II: Topical Studies in*  
2 *Oceanography*, 45, 2195–2223, [https://doi.org/10.1016/S0967-0645\(98\)00068-X](https://doi.org/10.1016/S0967-0645(98)00068-X), 1998.
- 3 Dang, C., Warren, S. G., Fu, Q., Doherty, S. J., Sturm, M., and Su, J.: Measurements of light-absorbing  
4 particles in snow across the Arctic, North America, and China: Effects on surface albedo, 122, 10,149–  
5 10,168, <https://doi.org/10.1002/2017JD027070>, 2017.
- 6 Di Mauro, B.: A darker cryosphere in a warming world, *Nat. Clim. Chang.*, 10, 978–979,  
7 <https://doi.org/10.1038/s41558-020-0896-8>, 2020.
- 8 Di Mauro, B., Fava, F., Ferrero, L., Garzonio, R., Baccolo, G., Delmonte, B., and Colombo, R.: Mineral  
9 dust impact on snow radiative properties in the European Alps combining ground, UAV, and satellite  
10 observations: MINERAL DUST ON SNOW IN THE ALPS, *J. Geophys. Res. Atmos.*, 120, 6080–  
11 6097, <https://doi.org/10.1002/2015JD023287>, 2015.
- 12 Doherty, S. J., Warren, S. G., Grenfell, T. C., Clarke, A. D., and Brandt, R. E.: Light-absorbing impurities  
13 in Arctic snow, *Atmos. Chem. Phys.*, 10, 11647–11680, <https://doi.org/10.5194/acp-10-11647-2010>,  
14 2010.
- 15 Doherty, S. J., Dang, C., Hegg, D. A., Zhang, R., and Warren, S. G.: Black carbon and other light-  
16 absorbing particles in snow of central North America: Black carbon in North American snow, *J.*  
17 *Geophys. Res. Atmos.*, 119, 12,807–12,831, <https://doi.org/10.1002/2014JD022350>, 2014.
- 18 Domine, F.: Air-Snow Interactions and Atmospheric Chemistry, 297, 1506–1510,  
19 <https://doi.org/10.1126/science.1074610>, 2002.
- 20 D'Sa, E. J., Goes, J. I., Gomes, H., and Mouw, C.: Absorption and fluorescence properties of  
21 chromophoric dissolved organic matter of the eastern Bering Sea in the summer with special reference  
22 to the influence of a cold pool, *Biogeosciences*, 11, 3225–3244, [https://doi.org/10.5194/bg-11-3225-](https://doi.org/10.5194/bg-11-3225-2014)  
23 2014, 2014.
- 24 Dumont, M., Brun, E., Picard, G., Michou, M., Libois, Q., Petit, J.-R., Geyer, M., Morin, S., and Josse,  
25 B.: Contribution of light-absorbing impurities in snow to Greenland's darkening since 2009, *Nature*  
26 *Geosci.*, 7, 509–512, <https://doi.org/10.1038/ngeo2180>, 2014.
- 27 Fang, L., Bai, Z., Wei, S., Yanfen, H., Zongming, W., Kaishan, S., Dianwei, L., and Zhiming, L.: Sandy  
28 desertification change and its driving forces in western Jilin Province, North China, *Environ Monit*  
29 *Assess.*, 136, 379–390, <https://doi.org/10.1007/s10661-007-9693-3>, 2007.



- 1 Fellman, J. B., Hood, E., Raymond, P. A., Stubbins, A., and Spencer, R. G. M.: Spatial Variation in the  
2 Origin of Dissolved Organic Carbon in Snow on the Juneau Icefield, Southeast Alaska, *Environ. Sci.*  
3 *Technol.*, 49, 11492–11499, <https://doi.org/10.1021/acs.est.5b02685>, 2015.
- 4 Feng, L., Xu, J., Kang, S., Li, X., Li, Y., Jiang, B., and Shi, Q.: Chemical Composition of Microbe-  
5 Derived Dissolved Organic Matter in Cryoconite in Tibetan Plateau Glaciers: Insights from Fourier  
6 Transform Ion Cyclotron Resonance Mass Spectrometry Analysis, *Environ. Sci. Technol.*, 50, 13215–  
7 13223, <https://doi.org/10.1021/acs.est.6b03971>, 2016.
- 8 Feng, L., An, Y., Xu, J., and Kang, S.: Characteristics and sources of dissolved organic matter in a glacier  
9 in the northern Tibetan Plateau: differences between different snow categories, *Ann. Glaciol.*, 59, 31–  
10 40, <https://doi.org/10.1017/aog.2018.20>, 2018.
- 11 Flanner, M. G., Zender, C. S., Randerson, J. T., and Rasch, P. J.: Present-day climate forcing and response  
12 from black carbon in snow, *J. Geophys. Res.*, 112, D11202, <https://doi.org/10.1029/2006JD008003>,  
13 2007.
- 14 Fu, P., Kawamura, K., Chen, J., Qin, M., Ren, L., Sun, Y., Wang, Z., Barrie, L. A., Tachibana, E., Ding,  
15 A., and Yamashita, Y.: Fluorescent water-soluble organic aerosols in the High Arctic atmosphere, *Sci*  
16 *Rep.*, 5, 9845, <https://doi.org/10.1038/srep09845>, 2015.
- 17 Grannas, A. M., Jones, A. E., Dibb, J., Ammann, M., Anastasio, C., Beine, H. J., Bergin, M., Bottenheim,  
18 J., Boxe, C. S., Carver, G., Chen, G., Crawford, J. H., Domine, F., Frey, M. M., Guzman, M. I., Heard,  
19 D. E., Helmig, D., Hoffmann, M. R., Honrath, R. E., Huey, L. G., Hutterli, M., Jacobi, H. W., Klan, P.,  
20 Lefer, B., McConnell, J., Plane, J., Sander, R., Savarino, J., Shepson, P. B., Simpson, W. R., Sodeau,  
21 J. R., Weller, R., Wolff, E. W., and Zhu, T.: An overview of snow photochemistry: evidence,  
22 mechanisms and impacts, 45, <https://doi.org/10/fjqs2v>, 2007.
- 23 Groisman, P. Ya., Karl, T. R., and Knight, R. W.: Observed Impact of Snow Cover on the Heat Balance  
24 and the Rise of Continental Spring Temperatures, *Science*, 263, 198–200,  
25 <https://doi.org/10.1126/science.263.5144.198>, 1994.
- 26 Guo, J. and Hu, Y.: Spatiotemporal Variations in Satellite-Derived Vegetation Phenological Parameters  
27 in Northeast China, *Remote Sensing*, 14, 705, <https://doi.org/10.3390/rs14030705>, 2022.
- 28 Gustafsson, Ö., Kruså, M., Zencak, Z., Sheesley, R. J., Granat, L., Engström, E., Praveen, P. S., Rao, P.  
29 S. P., Leck, C., and Rodhe, H.: Brown Clouds over South Asia: Biomass or Fossil Fuel Combustion?,



- 1 Science, 323, 495–498, <https://doi.org/10.1126/science.1164857>, 2009.
- 2 Hansen, J. and Nazarenko, L.: Soot climate forcing via snow and ice albedos, Proceedings of the National  
3 Academy of Sciences, 101, 423–428, <https://doi.org/10.1073/pnas.2237157100>, 2004.
- 4 Hegg, D. A., Warren, S. G., Grenfell, T. C., Sarah J Doherty, and Clarke, A. D.: Sources of light-absorbing  
5 aerosol in arctic snow and their seasonal variation, Atmos. Chem. Phys., 10, 10923–10938,  
6 <https://doi.org/10.5194/acp-10-10923-2010>, 2010.
- 7 Helms, J. R., Stubbins, A., Perdue, E. M., Green, N. W., Chen, H., and Mopper, K.: Photochemical  
8 bleaching of oceanic dissolved organic matter and its effect on absorption spectral slope and  
9 fluorescence, Marine Chemistry, 155, 81–91, <https://doi.org/10.1016/j.marchem.2013.05.015>, 2013.
- 10 Hood, E., Battin, T. J., Fellman, J., O’Neel, S., and Spencer, R. G. M.: Storage and release of organic  
11 carbon from glaciers and ice sheets, Nature Geosci, 8, 91–96, <https://doi.org/10.1038/ngeo2331>, 2015.
- 12 Hotaling, S., Lutz, S., Dial, R. J., Anesio, A. M., Benning, L. G., Fountain, A. G., Kelley, J. L.,  
13 McCutcheon, J., Skiles, S. M., Takeuchi, N., and Hamilton, T. L.: Biological albedo reduction on ice  
14 sheets, glaciers, and snowfields, Earth-Science Reviews, 220, 103728,  
15 <https://doi.org/10.1016/j.earscirev.2021.103728>, 2021.
- 16 Huang, J., Fu, Q., Zhang, W., Wang, X., Zhang, R., Ye, H., and Warren, S. G.: Dust and Black Carbon in  
17 Seasonal Snow Across Northern China, Bull. Amer. Meteor. Soc., 92, 175–181,  
18 <https://doi.org/10.1175/2010BAMS3064.1>, 2011.
- 19 Huguet, A., Vacher, L., Relexans, S., Saubusse, S., Froidefond, J. M., and Parlanti, E.: Properties of  
20 fluorescent dissolved organic matter in the Gironde Estuary, Organic Geochemistry, 40, 706–719,  
21 <https://doi.org/10.1016/j.orggeochem.2009.03.002>, 2009.
- 22 Kothawala, D. N., Murphy, K. R., Stedmon, C. A., Weyhenmeyer, G. A., and Tranvik, L. J.: Inner filter  
23 correction of dissolved organic matter fluorescence: Correction of inner filter effects, Limnol.  
24 Oceanogr. Methods, 11, 616–630, <https://doi.org/10.4319/lom.2013.11.616>, 2013.
- 25 Kowalczuk, P., Stoń-Egiert, J., Cooper, W. J., Whitehead, R. F., and Durako, M. J.: Characterization of  
26 chromophoric dissolved organic matter (CDOM) in the Baltic Sea by excitation emission matrix  
27 fluorescence spectroscopy, Marine Chemistry, 96, 273–292,  
28 <https://doi.org/10.1016/j.marchem.2005.03.002>, 2005.
- 29 Lawaetz, A. J. and Stedmon, C. A.: Fluorescence Intensity Calibration Using the Raman Scatter Peak of



- 1 Water, *Appl Spectrosc*, 63, 936–940, <https://doi.org/10.1366/000370209788964548>, 2009.
- 2 Li, C., Yan, F., Kang, S., Yan, C., Hu, Z., Chen, P., Gao, S., Zhang, C., He, C., Kaspari, S., and Stubbins,  
3 A.: Carbonaceous matter in the atmosphere and glaciers of the Himalayas and the Tibetan plateau: An  
4 investigative review, *Environment International*, 146, 106281,  
5 <https://doi.org/10.1016/j.envint.2020.106281>, 2021a.
- 6 Li, Y., Kang, S., Zhang, X., Chen, J., Schmale, J., Li, X., Zhang, Y., Niu, H., Li, Z., Qin, X., He, X., Yang,  
7 W., Zhang, G., Wang, S., Shao, L., and Tian, L.: Black carbon and dust in the Third Pole glaciers:  
8 Revaluated concentrations, mass absorption cross-sections and contributions to glacier ablation,  
9 *Science of The Total Environment*, 789, 147746, <https://doi.org/10.1016/j.scitotenv.2021.147746>,  
10 2021b.
- 11 Lu, Z., Zhang, Q., and Streets, D. G.: Sulfur dioxide and primary carbonaceous aerosol emissions in  
12 China and India, 1996–2010, *Atmos. Chem. Phys.*, 11, 9839–9864, [https://doi.org/10.5194/acp-11-](https://doi.org/10.5194/acp-11-9839-2011)  
13 9839-2011, 2011.
- 14 McKnight, D. M., Boyer, E. W., Westerhoff, P. K., Doran, P. T., Kulbe, T., and Andersen, D. T.:  
15 Spectrofluorometric characterization of dissolved organic matter for indication of precursor organic  
16 material and aromaticity, 46, 38–48, <https://doi.org/10.4319/lo.2001.46.1.0038>, 2001.
- 17 McNeill, V. F., Grannas, A. M., Abbatt, J. P. D., Ammann, M., Ariya, P., Bartels-Rausch, T., Domine, F.,  
18 Donaldson, D. J., Guzman, M. I., Heger, D., Kahan, T. F., Klán, P., Masclin, S., Toubin, C., and Voisin,  
19 D.: Organics in environmental ices: sources, chemistry, and impacts, *Atmos. Chem. Phys.*, 12, 9653–  
20 9678, <https://doi.org/10.5194/acp-12-9653-2012>, 2012.
- 21 Meyer, T. and Wania, F.: Organic contaminant amplification during snowmelt, *Water Research*, 42, 1847–  
22 1865, <https://doi.org/10.1016/j.watres.2007.12.016>, 2008.
- 23 Mladenov, N., Alados-Arboledas, L., Olmo, F. J., Lyamani, H., Delgado, A., Molina, A., and Reche, I.:  
24 Applications of optical spectroscopy and stable isotope analyses to organic aerosol source  
25 discrimination in an urban area, *Atmospheric Environment*, 45, 1960–1969,  
26 <https://doi.org/10.1016/j.atmosenv.2011.01.029>, 2011.
- 27 Murphy, K. R., Stedmon, C. A., Waite, T. D., and Ruiz, G. M.: Distinguishing between terrestrial and  
28 autochthonous organic matter sources in marine environments using fluorescence spectroscopy,  
29 *Marine Chemistry*, 108, 40–58, <https://doi.org/10.1016/j.marchem.2007.10.003>, 2008.



- 1 Murphy, K. R., Hambly, A., Singh, S., Henderson, R. K., Baker, A., Stuetz, R., and Khan, S. J.: Organic  
2 Matter Fluorescence in Municipal Water Recycling Schemes: Toward a Unified PARAFAC Model,  
3 Environ. Sci. Technol., 45, 2909–2916, <https://doi.org/10.1021/es103015e>, 2011.
- 4 Murphy, K. R., Stedmon, C. A., Graeber, D., and Bro, R.: Fluorescence spectroscopy and multi-way  
5 techniques. PARAFAC, Anal. Methods, 5, 6557, <https://doi.org/10.1039/c3ay41160e>, 2013.
- 6 Niu, H., Kang, S., Lu, X., and Shi, X.: Distributions and light absorption property of water soluble organic  
7 carbon in a typical temperate glacier, southeastern Tibetan Plateau, Tellus B: Chemical and Physical  
8 Meteorology, 70, 1–15, <https://doi.org/10.1080/16000889.2018.1468705>, 2018.
- 9 Ohno, T.: Fluorescence Inner-Filtering Correction for Determining the Humification Index of Dissolved  
10 Organic Matter, Environ. Sci. Technol., 36, 742–746, <https://doi.org/10.1021/es0155276>, 2002.
- 11 Osburn, C. L., Handsel, L. T., Peierls, B. L., and Paerl, H. W.: Predicting Sources of Dissolved Organic  
12 Nitrogen to an Estuary from an Agro-Urban Coastal Watershed, Environ. Sci. Technol., 50, 8473–8484,  
13 <https://doi.org/10.1021/acs.est.6b00053>, 2016.
- 14 Painter, T. H., Barrett, A. P., Landry, C. C., Neff, J. C., Cassidy, M. P., Lawrence, C. R., McBride, K. E.,  
15 and Farmer, G. L.: Impact of disturbed desert soils on duration of mountain snow cover, Geophys. Res.  
16 Lett., 34, L12502, <https://doi.org/10.1029/2007GL030284>, 2007.
- 17 Painter, T. H., Seidel, F. C., Bryant, A. C., McKenzie Skiles, S., and Rittger, K.: Imaging spectroscopy  
18 of albedo and radiative forcing by light-absorbing impurities in mountain snow: RADIATIVE  
19 FORCING DUST/BC IN SNOW, J. Geophys. Res. Atmos., 118, 9511–9523,  
20 <https://doi.org/10.1002/jgrd.50520>, 2013.
- 21 Pokrovsky, O. M.: Quantitative Estimates of the Impact of the Most Important Factors on Global Climate  
22 Change over the Past 150 Years, Izv. Atmos. Ocean. Phys., 55, 1182–1188,  
23 <https://doi.org/10.1134/S0001433819090354>, 2019.
- 24 Pu, W., Wang, X., Wei, H., Zhou, Y., Shi, J., Hu, Z., Jin, H., and Chen, Q.: Properties of black carbon and  
25 other insoluble light-absorbing particles in seasonal snow of northwestern China, The Cryosphere, 11,  
26 1213–1233, <https://doi.org/10.5194/tc-11-1213-2017>, 2017.
- 27 Pu, W., Cui, J., Shi, T., Zhang, X., He, C., and Wang, X.: The remote sensing of radiative forcing by  
28 light-absorbing particles (LAPs) in seasonal snow over northeastern China, Atmos. Chem. Phys., 19,  
29 9949–9968, <https://doi.org/10.5194/acp-19-9949-2019>, 2019.



- 1 Pu, W., Shi, T., Cui, J., Chen, Y., Zhou, Y., and Wang, X.: Enhancement of snow albedo reduction and  
2 radiative forcing due to coated black carbon in snow, *The Cryosphere*, 15, 2255–2272,  
3 <https://doi.org/10.5194/tc-15-2255-2021>, 2021.
- 4 Qian, Y., Yasunari, T. J., Doherty, S. J., Flanner, M. G., Lau, W. K. M., Ming, J., Wang, H., Wang, M.,  
5 Warren, S. G., and Zhang, R.: Light-absorbing particles in snow and ice: Measurement and modeling  
6 of climatic and hydrological impact, *Adv. Atmos. Sci.*, 32, 64–91, [https://doi.org/10.1007/s00376-014-](https://doi.org/10.1007/s00376-014-0010-0)  
7 0010-0, 2015.
- 8 Sarangi, C., Qian, Y., Rittger, K., Ruby Leung, L., Chand, D., Bormann, K. J., and Painter, T. H.: Dust  
9 dominates high-altitude snow darkening and melt over high-mountain Asia, *Nat. Clim. Chang.*, 10,  
10 1045–1051, <https://doi.org/10.1038/s41558-020-00909-3>, 2020.
- 11 Seekell, D. A., Lapierre, J.-F., Ask, J., Bergström, A.-K., Deininger, A., Rodríguez, P., and Karlsson, J.:  
12 The influence of dissolved organic carbon on primary production in northern lakes, 60, 1276–1285,  
13 <https://doi.org/10.1002/lno.10096>, 2015.
- 14 Shamjad, P. M., Tripathi, S. N., Thamban, N. M., and Vreeland, H.: Refractive Index and Absorption  
15 Attribution of Highly Absorbing Brown Carbon Aerosols from an Urban Indian City-Kanpur, *Sci Rep*,  
16 6, 37735, <https://doi.org/10.1038/srep37735>, 2016.
- 17 Shi, T., Pu, W., Zhou, Y., Cui, J., Zhang, D., and Wang, X.: Albedo of Black Carbon-Contaminated Snow  
18 Across Northwestern China and the Validation With Model Simulation, 125, e2019JD032065,  
19 <https://doi.org/10.1029/2019JD032065>, 2020.
- 20 Shi, T., Cui, J., Chen, Y., Zhou, Y., Pu, W., Xu, X., Chen, Q., Zhang, X., and Wang, X.: Enhanced light  
21 absorption and reduced snow albedo due to internally mixed mineral dust in grains of snow, *Atmos.*  
22 *Chem. Phys.*, 21, 6035–6051, <https://doi.org/10.5194/acp-21-6035-2021>, 2021.
- 23 Skiles, S. M., Flanner, M., Cook, J. M., Dumont, M., and Painter, T. H.: Radiative forcing by light-  
24 absorbing particles in snow, *Nature Clim Change*, 8, 964–971, [https://doi.org/10.1038/s41558-018-](https://doi.org/10.1038/s41558-018-0296-5)  
25 0296-5, 2018.
- 26 Song, K., Shang, Y., Wen, Z., Jacinthe, P.-A., Liu, G., Lyu, L., and Fang, C.: Characterization of CDOM  
27 in saline and freshwater lakes across China using spectroscopic analysis, *Water Research*, 150, 403–  
28 417, <https://doi.org/10.1016/j.watres.2018.12.004>, 2019.
- 29 Stedmon, C. A. and Markager, S.: Resolving the variability in dissolved organic matter fluorescence in a



- 1 temperate estuary and its catchment using PARAFAC analysis, *Limnol. Oceanogr.*, 50, 686–697,  
2 <https://doi.org/10.4319/lo.2005.50.2.0686>, 2005.
- 3 Stedmon, C. A., Markager, S., and Bro, R.: Tracing dissolved organic matter in aquatic environments  
4 using a new approach to fluorescence spectroscopy, *Marine Chemistry*, 82, 239–254,  
5 [https://doi.org/10.1016/S0304-4203\(03\)00072-0](https://doi.org/10.1016/S0304-4203(03)00072-0), 2003.
- 6 Stedmon, C. A., Thomas, D. N., Granskog, M., Kaartokallio, H., Papadimitriou, S., and Kuosa, H.:  
7 Characteristics of Dissolved Organic Matter in Baltic Coastal Sea Ice: Allochthonous or  
8 Autochthonous Origins?, *Environ. Sci. Technol.*, 41, 7273–7279, <https://doi.org/10.1021/es071210f>,  
9 2007.
- 10 Usha, K. H., Nair, V. S., and Babu, S. S.: Modeling of aerosol induced snow albedo feedbacks over the  
11 Himalayas and its implications on regional climate, *Clim Dyn*, 54, 4191–4210,  
12 <https://doi.org/10.1007/s00382-020-05222-5>, 2020.
- 13 Vione, D., Colombo, N., Said-Pullicino, D., Bocchiola, D., Confortola, G., Salerno, F., Viviano, G.,  
14 Fratianni, S., Martin, M., Godone, D., and Freppaz, M.: Seasonal variations in the optical  
15 characteristics of dissolved organic matter in glacial pond water, *Science of The Total Environment*,  
16 759, 143464, <https://doi.org/10.1016/j.scitotenv.2020.143464>, 2021.
- 17 Voisin, D., Jaffrezo, J.-L., Houdier, S., Barret, M., Cozic, J., King, M. D., France, J. L., Reay, H. J.,  
18 Grannas, A., Kos, G., Ariya, P. A., Beine, H. J., and Domine, F.: Carbonaceous species and humic like  
19 substances (HULIS) in Arctic snowpack during OASIS field campaign in Barrow, 117,  
20 <https://doi.org/10.1029/2011JD016612>, 2012.
- 21 Wang, J., Wang, Y., Yan, C., and Qi, Y.: 1:100,000 desert (sand) distribution dataset in China, edited by:  
22 National Tibetan Plateau Data Center, National Tibetan Plateau Data Center,  
23 <https://doi.org/10.3972/westdc.006.2013.db>, 2013a.
- 24 Wang, R., Tao, S., Balkanski, Y., Ciais, P., Boucher, O., Liu, J., Piao, S., Shen, H., Vuolo, M. R., Valari,  
25 M., Chen, H., Chen, Y., Cozic, A., Huang, Y., Li, B., Li, W., Shen, G., Wang, B., and Zhang, Y.:  
26 Exposure to ambient black carbon derived from a unique inventory and high-resolution model, *Proc.*  
27 *Natl. Acad. Sci. U.S.A.*, 111, 2459–2463, <https://doi.org/10.1073/pnas.1318763111>, 2014a.
- 28 Wang, X., Doherty, S. J., and Huang, J.: Black carbon and other light-absorbing impurities in snow across  
29 Northern China: LIGHT-ABSORBING IMPURITIES IN SNOW, *J. Geophys. Res. Atmos.*, 118,



- 1 1471–1492, <https://doi.org/10.1029/2012JD018291>, 2013b.
- 2 Wang, X., Xu, B., and Ming, J.: An overview of the studies on black carbon and mineral dust deposition  
3 in snow and ice cores in East Asia, *J Meteorol Res*, 28, 354–370, [https://doi.org/10.1007/s13351-014-](https://doi.org/10.1007/s13351-014-4005-7)  
4 4005-7, 2014b.
- 5 Wang, X., Pu, W., Shi, J., Bi, J., Zhou, T., Zhang, X., and Ren, Y.: A comparison of the physical and  
6 optical properties of anthropogenic air pollutants and mineral dust over Northwest China, *J Meteorol*  
7 *Res*, 29, 180–200, <https://doi.org/10.1007/s13351-015-4092-0>, 2015.
- 8 Wang, X., Pu, W., Ren, Y., Zhang, X., Zhang, X., Shi, J., Jin, H., Dai, M., and Chen, Q.: Observations  
9 and model simulations of snow albedo reduction in seasonal snow due to insoluble light-absorbing  
10 particles during 2014 Chinese survey, *Atmos. Chem. Phys.*, 17, 2279–2296,  
11 <https://doi.org/10.5194/acp-17-2279-2017>, 2017.
- 12 Wang, X., Bai, X., Ma, L., He, C., Jiang, H., Sheng, L., and Luo, W.: Snow depths' impact on soil  
13 microbial activities and carbon dioxide fluxes from a temperate wetland in Northeast China, *Sci Rep*,  
14 10, 8709, <https://doi.org/10.1038/s41598-020-65569-x>, 2020.
- 15 Warren, S. and Wiscombe, W.: A Model for the Spectral Albedo of Snow. II: Snow Containing  
16 Atmospheric Aerosols, *Journal of The Atmospheric Sciences - J ATMOS SCI*, 37, 2734–2745,  
17 [https://doi.org/10.1175/1520-0469\(1980\)037<2734:AMFTSA>2.0.CO;2](https://doi.org/10.1175/1520-0469(1980)037<2734:AMFTSA>2.0.CO;2), 1980.
- 18 Wen, H., Zhou, Y., Xu, X., Wang, T., Chen, Q., Chen, Q., Li, W., Wang, Z., Huang, Z., Zhou, T., Shi, J.,  
19 Bi, J., Ji, M., and Wang, X.: Water-soluble brown carbon in atmospheric aerosols along the transport  
20 pathway of Asian dust: Optical properties, chemical compositions, and potential sources, *Science of*  
21 *The Total Environment*, 789, 147971, <https://doi.org/10.1016/j.scitotenv.2021.147971>, 2021.
- 22 Wu, D., Shi, T., Niu, X., Chen, Z., Cui, J., Chen, Y., Zhang, X., Liu, J., Ji, M., Wang, X., and Pu, W.:  
23 Seasonal to sub-seasonal variations of the Asian Tropopause Aerosols Layer affected by the deep  
24 convection, surface pollutants and precipitation, *Journal of Environmental Sciences*, 114, 53–65,  
25 <https://doi.org/10.1016/j.jes.2021.07.022>, 2022.
- 26 Wu, D., Liu, J., Wang, T., Niu, X., Chen, Z., Wang, D., Zhang, X., Ji, M., Wang, X., and Pu, W.: Applying  
27 a dust index over North China and evaluating the contribution of potential factors to its distribution,  
28 *Atmospheric Research*, 254, 105515, <https://doi.org/10.1016/j.atmosres.2021.105515>, 2021.
- 29 Wu, G., Ram, K., Fu, P., Wang, W., Zhang, Y., Liu, X., Stone, E. A., Pradhan, B. B., Dangol, P. M.,



- 1 Panday, A. K., Wan, X., Bai, Z., Kang, S., Zhang, Q., and Cong, Z.: Water-Soluble Brown Carbon in  
2 Atmospheric Aerosols from Godavari (Nepal), a Regional Representative of South Asia, *Environ. Sci.*  
3 *Technol.*, 53, 3471–3479, <https://doi.org/10.1021/acs.est.9b00596>, 2019.
- 4 Wu, G., Wan, X., Ram, K., Li, P., Liu, B., Yin, Y., Fu, P., Loewen, M., Gao, S., Kang, S., Kawamura, K.,  
5 Wang, Y., and Cong, Z.: Light absorption, fluorescence properties and sources of brown carbon  
6 aerosols in the Southeast Tibetan Plateau, *Environmental Pollution*, 257, 113616,  
7 <https://doi.org/10.1016/j.envpol.2019.113616>, 2020.
- 8 Xie, X., Liu, X., Che, H., Xie, X., Li, X., Shi, Z., Wang, H., Zhao, T., and Liu, Y.: Radiative feedbacks  
9 of dust in snow over eastern Asia in CAM4-BAM, *Atmos. Chem. Phys.*, 18, 12683–12698,  
10 <https://doi.org/10.5194/acp-18-12683-2018>, 2018.
- 11 Xin, J., Gong, C., Liu, Z., Cong, Z., Gao, W., Song, T., Pan, Y., Sun, Y., Ji, D., Wang, L., Tang, G., and  
12 Wang, Y.: The observation-based relationships between PM<sub>2.5</sub> and AOD over China, 121, 10,701-  
13 10,716, <https://doi.org/10.1002/2015JD024655>, 2016.
- 14 Yamashita, Y., Jaffé, R., Maie, N., and Tanoue, E.: Assessing the dynamics of dissolved organic matter  
15 (DOM) in coastal environments by excitation emission matrix fluorescence and parallel factor analysis  
16 (EEM-PARAFAC), 53, 1900–1908, <https://doi.org/10.4319/lo.2008.53.5.1900>, 2008.
- 17 Yan, F., Kang, S., Li, C., Zhang, Y., Qin, X., Li, Y., Zhang, X., Hu, Z., Chen, P., Li, X., Qu, B., and  
18 Sillanpää, M.: Concentration, sources and light absorption characteristics of dissolved organic carbon  
19 on a medium-sized valley glacier, northern Tibetan Plateau, *The Cryosphere*, 10, 2611–2621,  
20 <https://doi.org/10.5194/tc-10-2611-2016>, 2016.
- 21 Zhang, R., Hegg, D. A., Huang, J., and Fu, Q.: Source attribution of light-absorbing impurities in seasonal  
22 snow across northern China, *Radiation/Atmospheric Modelling/Troposphere/Physics (physical*  
23 *properties and processes)*, <https://doi.org/10.5194/acpd-13-2155-2013>, 2013.
- 24 Zhang, Y., van Dijk, M. A., Liu, M., Zhu, G., and Qin, B.: The contribution of phytoplankton degradation  
25 to chromophoric dissolved organic matter (CDOM) in eutrophic shallow lakes: Field and experimental  
26 evidence, *Water Research*, 43, 4685–4697, <https://doi.org/10.1016/j.watres.2009.07.024>, 2009.
- 27 Zhang, Y., Kang, S., Cong, Z., Schmale, J., Sprenger, M., Li, C., Yang, W., Gao, T., Sillanpää, M., Li, X.,  
28 Liu, Y., Chen, P., and Zhang, X.: Light-absorbing impurities enhance glacier albedo reduction in the  
29 southeastern Tibetan plateau: Light-Absorbing Impurities in Snow, *J. Geophys. Res. Atmos.*, 122,



- 1 6915–6933, <https://doi.org/10.1002/2016JD026397>, 2017.
- 2 Zhang, Y., Kang, S., Sprenger, M., Cong, Z., Gao, T., Li, C., Tao, S., Li, X., Zhong, X., Xu, M., Meng,  
3 W., Neupane, B., Qin, X., and Sillanpää, M.: Black carbon and mineral dust in snow cover on the  
4 Tibetan Plateau, *The Cryosphere*, 12, 413–431, <https://doi.org/10.5194/tc-12-413-2018>, 2018.
- 5 Zhang, Y., Kang, S., Gao, T., Sprenger, M., Dou, T., Han, W., Zhang, Q., Sun, S., Du, W., Chen, P., Guo,  
6 J., Cui, X., and Sillanpää, M.: Dissolved organic carbon in Alaskan Arctic snow: concentrations, light-  
7 absorption properties, and bioavailability, *Tellus B: Chemical and Physical Meteorology*, 72, 1–19,  
8 <https://doi.org/10.1080/16000889.2020.1778968>, 2020.
- 9 Zhao, C., Hu, Z., Qian, Y., Ruby Leung, L., Huang, J., Huang, M., Jin, J., Flanner, M. G., Zhang, R.,  
10 Wang, H., Yan, H., Lu, Z., and Streets, D. G.: Simulating black carbon and dust and their radiative  
11 forcing in seasonal snow: a case study over North China with field campaign measurements, *Atmos.*  
12 *Chem. Phys.*, 14, 11475–11491, <https://doi.org/10.5194/acp-14-11475-2014>, 2014.
- 13 Zhao, Y., Xu, X., Huang, W., Wang, Y., Xu, Y., Chen, H., and Kang, Z.: Trends in observed mean and  
14 extreme precipitation within the Yellow River Basin, China, *Theor Appl Climatol*, 136, 1387–1396,  
15 <https://doi.org/10.1007/s00704-018-2568-4>, 2019.
- 16 Zhou, L., Zhou, Y., Hu, Y., Cai, J., Liu, X., Bai, C., Tang, X., Zhang, Y., Jang, K.-S., Spencer, R. G. M.,  
17 and Jeppesen, E.: Microbial production and consumption of dissolved organic matter in glacial  
18 ecosystems on the Tibetan Plateau, *Water Research*, 160, 18–28,  
19 <https://doi.org/10.1016/j.watres.2019.05.048>, 2019a.
- 20 Zhou, Y., Shi, K., Zhang, Y., Jeppesen, E., Liu, X., Zhou, Q., Wu, H., Tang, X., and Zhu, G.: Fluorescence  
21 peak integration ratio IC:IT as a new potential indicator tracing the compositional changes in  
22 chromophoric dissolved organic matter, 11, 2017.
- 23 Zhou, Y., Wen, H., Liu, J., Pu, W., Chen, Q., and Wang, X.: The optical characteristics and sources of  
24 chromophoric dissolved organic matter (CDOM) in seasonal snow of northwestern China, *The*  
25 *Cryosphere*, 13, 157–175, <https://doi.org/10.5194/tc-13-157-2019>, 2019b.
- 26 Zhou, Y., West, C. P., Hettiyadura, A. P. S., Niu, X., Wen, H., Cui, J., Shi, T., Pu, W., Wang, X., and  
27 Laskin, A.: Measurement report: Molecular composition, optical properties, and radiative effects of  
28 water-soluble organic carbon in snowpack samples from northern Xinjiang, China, *Atmos. Chem.*  
29 *Phys.*, 21, 8531–8555, <https://doi.org/10.5194/acp-21-8531-2021>, 2021.



- 1 Zhou, Y., West, C. P., Hettiyadura, A. P. S., Pu, W., Shi, T., Niu, X., Wen, H., Cui, J., Wang, X., and  
2 Laskin, A.: Molecular Characterization of Water-Soluble Brown Carbon Chromophores in Snowpack  
3 from Northern Xinjiang, China, *Environ. Sci. Technol.*, [acs.est.1c07972](https://doi.org/10.1021/acs.est.1c07972),  
4 <https://doi.org/10.1021/acs.est.1c07972>, 2022.
- 5 Zsolnay, A., Baigar, E., Jimenez, M., Steinweg, B., and Saccomandi, F.: Differentiating with fluorescence  
6 spectroscopy the sources of dissolved organic matter in soils subjected to drying, 38, 45–50,  
7 [https://doi.org/10.1016/S0045-6535\(98\)00166-0](https://doi.org/10.1016/S0045-6535(98)00166-0), 1999.
- 8 Zatko, M. C., Grenfell, T. C., Alexander, B., Doherty, S. J., Thomas, J. L., and Yang, X.: The influence  
9 of snow grain size and impurities on the vertical profiles of actinic flux and associated  
10 NO<sub>x</sub> emissions on the Antarctic and Greenland ice sheets, *Atmos. Chem.  
11 Phys.*, 13, 3547–3567, <https://doi.org/10.5194/acp-13-3547-2013>, 2013.